Causal IIR Audio Precompensator Filters Subject to Quadratic Constraints

Simon Widmark, *Student Member, IEEE*

***Abstract*—Infinite impulse response (IIR) Wiener precompensator design, with constraints on causality, is here also extended to incorporate general quadratic constraints. A method for finding a linear quadratic optimal, causal discrete-time multiple-input multiple-output filter subject to a set of user defined constraints is proposed and analyzed. A method for designing causal filters subject to constraints on the power gains in a large number of small frequency intervals is also proposed. The resulting set of methods provide constrained stable IIR filters with optimal parameterization. Compared to finite impulse response Wiener filtering, the computational complexity is much lower; and compared to noncausal frequency domain designs, we gain control of the time-domain properties of the compensated system. The design methods are applied to a room compensation audio problem subject to filter power gain constraint(s) and are compared to a corresponding noncausal per-frequency method. The results are presented with audio filtering and sound field control as main motivating applications but the methods extend to other areas of linear feedforward controller design and Wiener filtering.**

***Index Terms*—Signal processing algorithms, optimization methods, acoustic signal processing, IIR filters.**

I. Introduction

In THIS paper, we present a method for incorporating quadratic constraints into a pre-existing theoretical framework that is capable of producing broadband causal filters with reduced computational effort as compared to the traditional Toeplitz structured solution. This provides the benefit that we may compute causal filters in many instances where delayed non-causal filters were previously the only numerically feasible option. That in turn enables greatly improved control over temporal properties such as delays and pre-ringing in the compensated system.

Linear digital precompensation filters can be used for several purposes in audio systems: loudspeaker equalization, cross-talk cancellation between audio channels, up-mixing of channels to a set of loudspeakers, compensation of the room acoustics and as a tool for sound field control.

The design of such filters has traditionally mostly been formulated as a non-causal Wiener precompensator design problem. It is solved by mean square error minimization point-wise in the frequency domain, as a regularized inverse of the matrix of acoustic transfer functions that define the system. Unfortunately, these solutions often have unsatisfactory time-domain properties: The remaining errors of the compensated impulse responses will have components before the start of a desired impulse response (pre-ringing) and also after it (post-ringing). While both effects are partially masked by auditory masking effects [1], pre-ringing is usually much more noticeable, and may give the sound an undesirable quality. A non-causal frequency domain Wiener design cannot control such effects.

Causal Wiener designs of pre-compensator filters, which are in focus in the present paper, have the desirable property that the duration of pre-ringing in compensated impulse responses is limited by the causality constraint that is imposed on the solution. Furthermore, design under a causality constraint will provide tight control of the processing delay, which may be important in some applications such as e.g. duplex communication or music recording and mixing.

It would be useful to be able to perform a causal audio pre-compensator design subject to quadratic constraints. For example, the power to loudspeakers should be within prescribed bounds, the generated pressure in a spatial region should be limited, or the deviation from a target system response should have limited magnitude. Methods for adding quadratic constraints to Wiener pre-compensator designs are known for two special cases discussed below:

1) When using finite impulse response (FIR) model and filter structures, see e.g., [2, Sec. 4] and
2) When using non-causal Wiener filters [3].

A convex optimization formulation can be used in both cases. However, no method exist to add quadratic constraints to causal infinite impulse response (IIR) polynomial matrix Wiener filters and this problem is not trivial to formulate in the convex optimization framework. The purpose of the present paper is to solve this problem, using a Lagrangian approach, to illustrate the properties of the solution and relate these to constrained non-causal filtering.

Causal FIR pre-compensation filters for audio can be derived subject to a host of different constraints using a block Toeplitz structure for system modelling, (see e.g. [4]) along with e.g. convex optimization theory (see e.g. [5]). An example where causal FIR filters for personal audio are designed under filter power gain constraints can be found in [2]. Unfortunately, design of causal FIR filters based on system descriptions of FIR filtered signals is normally associated with computationally taxing

Manuscript received November 9, 2017; revised February 22, 2018 and April 25, 2018; accepted May 6, 2018. Date of publication May 28, 2018; date of current version July 10, 2018. This work was supported in part by the Swedish Research Council under Contract 621-2014-5871 and in part by Knut and Alice Wallenberg Foundation. The associate editor coordinating the review of this manuscript and approving it for publication was Prof. Augusto Sarti.

The author is with the Signals and Systems Group, Uppsala University, Uppsala 751 21, Sweden, and also with Dirac Research AB, Uppsala 753 20, Sweden (e-mail: simon.widmark@angstrom.uu.se).

Digital Object Identifier 10.1109/TASLP.2018.2839355

large matrix inverses. For example, FIR approximations of the filter design examples in this paper would involve matrices with more than 1.9×10^{10} elements, and cannot be handled with reasonable memory requirements. Another problem related to the commonly used causal FIR filter design methods is that of choosing filter lengths. Longer filters typically generate better low-frequency performance of the compensated system while the dimensions of the matrix-to-be-inverted grows rapidly with the filter length. This trade-off complicates the FIR design problem.

In a non-causal Wiener solution, constraints such as those discussed in the present paper can be defined per frequency. The resulting quadratic optimization problem with quadratic constraints can, similarly to the causal FIR filter problems discussed above, be formulated and solved as a convex optimization problem, see [6], [3] by Betlehem and co-workers. Solving the filter design problem point-wise in the frequency domain avoids the problem of inverting unreasonably large matrices. This in turn somewhat alleviates the problem of choosing motivated filter lengths, but does not solve it completely.

The related problem of Wiener post-filtering under general constraints has been discussed by Michaeli and Eldar [7], [8].

Filter generation for audio pre-compensation problems has been extensively studied and has a long and rich history (see e.g. [9]). In broad terms, the methods for audio pre-compensation in the literature may be partitioned into two categories: analytical and numerical methods. In the former, we sort methods which are based on mathematical models of e.g. the sound field. Prominent examples drawn from the sound field synthesis literature are Wave Field Synthesis (WFS) [10] and Higher Order Ambisonics (HOA) [11], based on the Kirchoff-Helmholtz integral and on a decomposition of the sound field into a series of eigenfunctions, respectively. This class of methods often require highly specialized room and loudspeaker geometries due to their idealized nature. In the latter category, we sort measurement based methods, such as the multipoint mean square error minimization via least squares optimization (MMSE-LS) method, see e.g. [12]. This class of methods require very few assumptions regarding the physical reality in which it is implemented but may instead require a large number of measurements in order to adequately model the sound field at higher frequencies. These methods may also be susceptible to over-fitting to noisy model estimates.

In parallel with, and preceding much of, the research on audio pre-compensation filters, the rational matrix framework was developed and applied to active control problems [13], [14]. This particular parametrization, which is a measurement driven MMSE-LS approach, represents a computationally efficient and versatile design methodology when applied to audio pre-compensation problems. Yet it has been under-utilized since its first appearance in the audio research literature in the early 2000's [15].

The existing body of work on the Linear Quadratic design of causal and stable IIR filters for pre-compensation of linear systems reveals a powerful and versatile design framework based on matrix fraction descriptions [16] of linear systems, see e.g. [17]–[21]. This framework can be used for designing causal discrete-time Wiener filters for various problems [22], and also linear feed-forward pre-compensation filters designed to minimize quadratic criteria [23]–[25]. The linear quadratic feed-forward pre-compensator design problem can be shown to be dual to a specific type of Wiener filtering problem, namely deconvolution, or estimation of the input to a dynamic system [26]. The solutions to these two problems are therefore closely related [27].

This mathematical structure where matrices of polynomials represent a system of discrete-time filters or transfer functions (polynomial- and rational matrices), has proven to be both mathematically tractable and helpful for intuitive understanding of the properties of the resulting filters. Additionally, the filter parametrization is here not specified by the designer but is given by the design method itself, resulting in an optimal IIR filter parametrization. Although the polynomial matrix framework has many advantages, it is not yet explored how to explicitly incorporate quadratic constraints into the filter design.

In the present paper, the Lagrange multiplier method is utilized to include quadratic constraints in the design of causal IIR Wiener pre-compensation filters via the rational matrix framework. Although this filter optimization problem does not fall into the convex optimization framework (as will be made clear later), the Lagrange duality gap is zero since we can find a global minimizer to the primal problem. Single and multiple constraints on the filter power gain are derived as examples. A method for satisfying a dense set of frequency domain constraints, corresponding to the non-causal per-frequency constrained designs, is also presented. With the resulting set of methods, optimisation of causal filters subject to quadratic constraints is included into the theoretical framework for rational matrix Wiener filter design.

A. Outline of the Paper

The paper is structured as follows: The theoretical background and a succinct but general presentation of the constrained, causal filter design methodology are given in Section II. In Section III, the design method is elaborated and applied to a set of example problems, which are analysed and compared to each other: single constraint, multiple constraints, dense constraints in the frequency domain and the constrained non-causal solution. The conclusions drawn in the paper are summarized in Section IV. Derivations are found in Appendix A and B and details of the experimental set-up in Appendix C.

II. Constrained Causal IIR Wiener Design of MIMO Pre-Compensation Filters

A. Notation

Scalar quantities are, in this paper, denoted by lower case or capital letters, a, A. The integer t is used as a discrete time index. Polynomial matrices are denoted by capital, bold, italic letters $\boldsymbol{A}(q^{-1})$. The polynomial matrix elements are FIR filters, which are polynomials in the delay operator, q^{-1}, so that $q^{-1}y(t) = y(t-1)$ which corresponds to z^{-1} or $e^{-j\omega}$ in the frequency domain. The corresponding forward shift operator is q, $qy(t) = y(t+1)$ which corresponds to z or $e^{j\omega}$. Rational

matrices (matrices of rational transfer functions) are denoted by capital bold script letters, $\boldsymbol{\mathcal{A}}(q^{-1})$. The rational matrix can be seen as a matrix with IIR filters as elements.

Regular (constant) matrices and vectors are denoted by bold, capital and lower case letters, $\mathbf{A}$ and $\boldsymbol{a}$ respectively.

Matrix inverses are denoted $\mathbf{A}^{-1}$. Complex matrices can be complex conjugated, $\mathbf{A}^*$, transposed $\mathbf{A}^T$ and both, $\mathbf{A}^H$. A polynomial matrix subject to the conjugate operator, $\boldsymbol{A}_*(q)$, is complex conjugate transposed and any delay operators are replaced by their reciprocal: $\boldsymbol{A}_*(q)$ is found by substituting q for q^{-1} in $\boldsymbol{A}^H(q^{-1})$. Unless otherwise stated, polynomials are expressed in the backward shift operator, q^{-1}. Conjugate polynomial- and rational matrices therefore normally contain polynomials in the forward shift operator, q. The arguments q^{-1} or q will be omitted in some expressions where this can be done without introducing ambiguity. Matrix dimensions are denoted, for a matrix with R rows and C columns, as $R|C$. The degree of a polynomial matrix $\boldsymbol{A}$, i.e. the highest power of q or the lowest power of q^{-1} with a non-zero coefficient is denoted $n_{\boldsymbol{A}}$.

Definiteness and semi-definiteness of matrices is indicated by the symbols $\succ$ and $\succeq$ respectively, where $\mathbf{A} \succeq \mathbf{B} \iff \mathbf{A} - \mathbf{B} \succeq 0$, i.e., if $\mathbf{A} - \mathbf{B}$ is a positive semi-definite matrix.

B. The Audio Pre-Compensation Problem

Assume that a linear electro-acoustical system with N loudspeakers and M control points is described correctly and completely by a rational matrix $\boldsymbol{\mathcal{H}}(q^{-1})$. Each column of the $M|N$ matrix $\boldsymbol{\mathcal{H}}(q^{-1})$ contains stable transfer function models from the input to one loudspeaker to the sound pressure at a set of design positions. Every row thus contains the transfer function models to one design point from all loudspeakers.

Before a signal is amplified and replayed by the loudspeakers, it is pre-processed by an $N|1$ rational filter vector $\boldsymbol{\mathcal{R}}_l(q^{-1})$. Each element of the filter vector $\boldsymbol{\mathcal{R}}_l(q^{-1})$ thus holds the IIR filter which is used to pre-processes the signal that is later fed to the corresponding amplifier-loudspeaker combination. We can use the assumed linearity to generate a filter for a situation where we have more than one input signal by adding the result of l signals processed by l associated filters, the dimensions of the filter matrix $\boldsymbol{\mathcal{R}}(q^{-1}) = [\boldsymbol{\mathcal{R}}_1(q^{-1}) \cdots \boldsymbol{\mathcal{R}}_l(q^{-1})]$ then becomes $N|l$. We model the input signal to the filter matrix as a white[1] noise and will refer to it by the $l|1$ vector $\boldsymbol{r}(t)$, with zero mean and covariance matrix $E\{\boldsymbol{r}(t)\boldsymbol{r}^T(t)\} = \varrho\mathbf{P}$ of full rank, where $\varrho > 0$ is a scalar scaling factor. The notation $E\{\cdot\}$ here represents the expectation operator with respect to the statistics of $\boldsymbol{r}(t)$.

The output from the filter-system combination is contained in the $M|l$ vector $\boldsymbol{z}(t)$. An $M|l$ polynomial matrix, $\boldsymbol{D}(q^{-1})$, is used to describe the *desired* (or *target*) behaviour of the pre-compensated system. The desired transfer functions should include a common modelling delay, q^{-d}, greater than the largest path delay of $\boldsymbol{\mathcal{H}}(q^{-1})$. Increasing the modelling delay increases the achievable spectral fidelity of the solution, but also generally increases the amount of perceptible pre-ringing in the impulse responses of the compensated system $\boldsymbol{\mathcal{H}}(q^{-1})\boldsymbol{\mathcal{R}}(q^{-1})$.

[1]Coloured stochastic signals are also admissible inputs. The input signal $\boldsymbol{r}(t)$ is then modelled as $\boldsymbol{r}(t) = \mathcal{M}(q^{-1})\boldsymbol{e}(t)$ where $\mathcal{M}$ is an autoregressive moving average (ARMA) model and $\boldsymbol{e}(t)$ is a white input noise vector. This approach is e.g. utilized with an autoregressive model in [25].

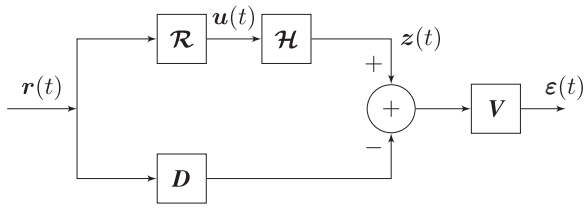

Fig. 1. A pre-compensated electro-acoustical system with desired response $\boldsymbol{D}(q^{-1})$, error vector $\boldsymbol{\varepsilon}(t)$, pre-compensator output vector $\boldsymbol{u}(t)$ and pre-compensated system output vector $\boldsymbol{z}(t)$.

We can now specify the deviation between the actual system behaviour and the desired system behaviour as

$$\boldsymbol{\varepsilon}(t) = \boldsymbol{V}(q^{-1})\left(\boldsymbol{\mathcal{H}}(q^{-1})\boldsymbol{\mathcal{R}}(q^{-1}) - \boldsymbol{D}(q^{-1})\right)\boldsymbol{r}(t). \quad (1)$$

Above, we also introduce an $M|M$ system reproduction error weighting matrix, $\boldsymbol{V}(q^{-1})$ of full rank with which we can assign more or less importance to the error at certain spectral bands and control points. The audio pre-compensation problem at hand is illustrated in Fig. 1.

In Fig. 1, we also introduce the variables $\boldsymbol{u}(t)$ representing the output from the pre-compensator to be designed, $\boldsymbol{u}(t) = \boldsymbol{\mathcal{R}}(q^{-1})\boldsymbol{r}(t)$, and $\boldsymbol{z}(t)$ representing the output from the compensated system $\boldsymbol{z}(t) = \boldsymbol{\mathcal{H}}(q^{-1})\boldsymbol{u}(t)$.

There are many important aspects to the audio pre-compensation problem where simple minimization of the expected value of $\|\boldsymbol{\varepsilon}(t)\|_2^2$ is not sufficient. For instance, the loudspeakers may have some constraints associated with them, e.g. in that they are designed for a limited portion of the audible spectra only. Other interesting constraints include those on the magnitude of the target error at a subset of the design points. These constraints can be formulated using functions in which the pre-compensator $\boldsymbol{\mathcal{R}}(q^{-1})$ enters quadratically. Although important to the audio pre-compensation problem, such constraints have previously not been included in the set of known filter derivation techniques using the rational matrix framework.

C. Rational Matrix Filter Optimization With Quadratic Criteria and Power Spectral Density Constraints

In the following, a general presentation and motivation of the filter derivation technique discussed in the paper is given. This technique will be exemplified by more specific use cases in the subsequent section.

Assume that an optimization problem is given on the form

$$\min_{\boldsymbol{\mathcal{R}}} . \quad J(\boldsymbol{\mathcal{R}}) = E\left\{\boldsymbol{x}^T(\boldsymbol{\mathcal{R}}, t)\,\boldsymbol{x}(\boldsymbol{\mathcal{R}}, t)\right\}$$
$$\text{s.t.} \quad C(\boldsymbol{\mathcal{R}}) = E\left\{\boldsymbol{y}^T(\boldsymbol{\mathcal{R}}, t)\,\boldsymbol{y}(\boldsymbol{\mathcal{R}}, t)\right\} - e_c \leq 0. \quad (2)$$

The column vectors $\boldsymbol{x}(\boldsymbol{\mathcal{R}}, t)$ and $\boldsymbol{y}(\boldsymbol{\mathcal{R}}, t)$ above are instances of time domain signals in discrete time, described by models of linear, stable and time invariant systems in the form of polynomial- or rational matrices in the backward shift operator. They are assumed to be driven by a stationary noise signal vector $\boldsymbol{r}(t)$. Note that the expressions (2) in the optimization problem will

be scalar. The constraint value e_c is a scalar positive constant. Included in our feed-forward signal paths is also a causal, rational and stable matrix, $\boldsymbol{\mathcal{R}}(q^{-1})$, which we strive to optimize according to (2). It is assumed that the rational matrix $\boldsymbol{\mathcal{R}}$ affects both $\boldsymbol{x}$ and $\boldsymbol{y}$ linearly and that the constraint can be attained with inequality. Note that while the controller matrix $\boldsymbol{\mathcal{R}}(q^{-1})$ enters the problem in a linear-quadratic fashion, the individual filter coefficients contained in $\boldsymbol{\mathcal{R}}$ will generally not enter $\boldsymbol{x}$ nor $\boldsymbol{y}$ linearly, as $\boldsymbol{\mathcal{R}}$ describes a set of IIR filters. Further, the design process itself defines the optimal number of coefficients needed to solve the problem, and so the dimension and structure of the parameter space is not defined by the user. Finally, also note that the controller-to-be-designed is given as a matrix of rational functions in the delay operator and does therefore not fall into the convex optimization framework.

There is a crucial property that will provide a way forward for the problem at hand. If we can find the global minimum with respect to our controller for the Lagrange objective function associated to the problem, then the Lagrange multiplier formulation can be utilized to solve (2). Further, as this would also imply that no duality gap is present, we can then use the Lagrange dual optimization to find a solution to our problem. A general proof for this, generalized to multiple constraints, is included in Appendix A-A.

The Lagrange objective function is constructed by adding the constraint function $C(\boldsymbol{\mathcal{R}})$, multiplied by a scalar weight λ, to the original objective function,

$$\mathcal{L}\left(\boldsymbol{\mathcal{R}},\lambda\right) = E\left\{\boldsymbol{x}^T\left(\boldsymbol{\mathcal{R}},t\right)\boldsymbol{x}(\boldsymbol{\mathcal{R}},t) + \lambda\left(\boldsymbol{y}^T\left(\boldsymbol{\mathcal{R}},t\right)\boldsymbol{y}(\boldsymbol{\mathcal{R}},t) - e_c\right)\right\}. \tag{3}$$

The weight λ is a penalty on the deviation between the square Euclidian norm of the signal $\boldsymbol{y}(t)$ and the constraint level e_c.

The optimal solution to the constrained problem (2) is then the pair $\boldsymbol{\mathcal{R}}_{opt}, \lambda_{opt}$ where $\boldsymbol{\mathcal{R}}_{opt}$ (uniquely) minimizes the Lagrange function (3) and λ_{opt} maximizes the dual function

$$\mathcal{G}(\lambda) = \min_{\boldsymbol{\mathcal{R}}}. \quad \mathcal{L}\left(\boldsymbol{\mathcal{R}},\lambda\right). \tag{4}$$

For a proof: see Appendix A-A.

Our method will therefore be to search for the multiplier λ that maximizes (4) together with the pre-compensator $\boldsymbol{\mathcal{R}}(q^{-1})$ that minimizes (3). The Lagrange dual function is a concave function in the Lagrange multiplier(s) and efficient numerical methods exist for finding the optimal value for λ. A general method for deriving a causal and stable linear controller $\boldsymbol{\mathcal{R}}(q^{-1})$ that uniquely minimizes (3) for a given λ is outlined below. This problem is thus solved repeatedly, while iteratively maximizing (4) w.r.t. λ.

Minimizing $\mathcal{L}$ by Imposing Orthogonality in the Frequency Domain: We will now utilize the method proposed in [24] to uniquely minimize $\mathcal{L}(\boldsymbol{\mathcal{R}},\lambda)$ for a given λ. Much of the details will here be suppressed in order to keep the discussion brief, mathematical specifics can be found in [24] and also in the examples in Section III and in Appendix A-B.

Add to the causal and stable controller, $\boldsymbol{\mathcal{R}}(q^{-1})$, a causal and stable variation (perturbation) transfer function, $\boldsymbol{\mathcal{T}}(q^{-1})$. This addition might be beneficial, i.e. reduce the value of the Lagrange function, or detrimental, i.e. increase the value of the Lagrange function. Our goal in designing the controller $\boldsymbol{\mathcal{R}}$ is to choose it so that *no* addition $\boldsymbol{\mathcal{T}}$ can be beneficial, thus guaranteeing that our controller $\boldsymbol{\mathcal{R}}$ is the optimal causal and stable solution.

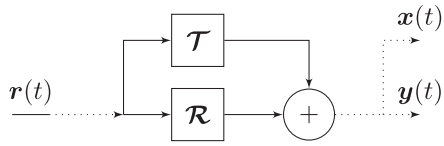

Fig. 2. Block diagram representation of the controller and variation. Dotted lines represent so far unspecified linear transfer paths of the system.

We use the assumed linear influence of $\boldsymbol{\mathcal{R}}+\boldsymbol{\mathcal{T}}$ on $\boldsymbol{x}(t)$ and $\boldsymbol{y}(t)$ in (3) to additively partition these signal vectors as

$$\begin{aligned}\boldsymbol{x}(\boldsymbol{\mathcal{R}}+\boldsymbol{\mathcal{T}},t) &= \boldsymbol{x}\left(\boldsymbol{\mathcal{R}},t\right) + \boldsymbol{x}\left(\boldsymbol{\mathcal{T}},t\right)\\ \boldsymbol{y}(\boldsymbol{\mathcal{R}}+\boldsymbol{\mathcal{T}},t) &= \boldsymbol{y}\left(\boldsymbol{\mathcal{R}},t\right) + \boldsymbol{y}\left(\boldsymbol{\mathcal{T}},t\right),\end{aligned} \tag{5}$$

where $\boldsymbol{x}(\boldsymbol{\mathcal{T}},t)$ and $\boldsymbol{y}(\boldsymbol{\mathcal{T}},t)$ are the additive contributions to $\boldsymbol{x}(t)$ and $\boldsymbol{y}(t)$ respectively, obtained by adding the output of the perturbation filter $\boldsymbol{\mathcal{T}}(q^{-1})$ to the output of $\boldsymbol{\mathcal{R}}(q^{-1})$ (see Fig. 2). We can now structure $\mathcal{L}(\boldsymbol{\mathcal{R}}+\boldsymbol{\mathcal{T}},\lambda)$ (in which both $\boldsymbol{x}(\boldsymbol{\mathcal{R}}+\boldsymbol{\mathcal{T}},t)$ and $\boldsymbol{y}(\boldsymbol{\mathcal{R}}+\boldsymbol{\mathcal{T}},t)$ are squared) based on all permutations of $\boldsymbol{\mathcal{R}}, \boldsymbol{\mathcal{R}}^T, \boldsymbol{\mathcal{T}}$ and $\boldsymbol{\mathcal{T}}^T$,

$$\begin{aligned}\mathcal{L}\left(\boldsymbol{\mathcal{R}}+\boldsymbol{\mathcal{T}},\lambda\right) &= \mathcal{L}_1(\boldsymbol{\mathcal{R}}^T,\boldsymbol{\mathcal{R}},\lambda) + \mathcal{L}_2(\boldsymbol{\mathcal{R}}^T,\boldsymbol{\mathcal{T}},\lambda)\\ &\quad + \mathcal{L}_3(\boldsymbol{\mathcal{T}}^T,\boldsymbol{\mathcal{R}},\lambda) + \mathcal{L}_4(\boldsymbol{\mathcal{T}}^T,\boldsymbol{\mathcal{T}},\lambda),\end{aligned} \tag{6}$$

where

$$\begin{aligned}&\mathcal{L}_1\left(\boldsymbol{\mathcal{R}}^T,\boldsymbol{\mathcal{R}},\lambda\right)\\ &\quad = E\left\{\boldsymbol{x}^T\left(\boldsymbol{\mathcal{R}},t\right)\boldsymbol{x}\left(\boldsymbol{\mathcal{R}},t\right) + \lambda\boldsymbol{y}^T\left(\boldsymbol{\mathcal{R}},t\right)\boldsymbol{y}\left(\boldsymbol{\mathcal{R}},t\right) - \lambda e_c\right\}\\ &\mathcal{L}_2\left(\boldsymbol{\mathcal{R}}^T,\boldsymbol{\mathcal{T}},\lambda\right) = \mathcal{L}_3\left(\boldsymbol{\mathcal{T}}^T,\boldsymbol{\mathcal{R}},\lambda\right)\\ &\mathcal{L}_3\left(\boldsymbol{\mathcal{T}}^T,\boldsymbol{\mathcal{R}},\lambda\right)\\ &\quad = E\left\{\boldsymbol{x}^T\left(\boldsymbol{\mathcal{T}},t\right)\boldsymbol{x}\left(\boldsymbol{\mathcal{R}},t\right) + \lambda\boldsymbol{y}^T\left(\boldsymbol{\mathcal{T}},t\right)\boldsymbol{y}\left(\boldsymbol{\mathcal{R}},t\right)\right\}\\ &\mathcal{L}_4\left(\boldsymbol{\mathcal{T}}^T,\boldsymbol{\mathcal{T}},\lambda\right)\\ &\quad = E\left\{\boldsymbol{x}^T\left(\boldsymbol{\mathcal{T}},t\right)\boldsymbol{x}\left(\boldsymbol{\mathcal{T}},t\right) + \lambda\boldsymbol{y}^T\left(\boldsymbol{\mathcal{T}},t\right)\boldsymbol{y}\left(\boldsymbol{\mathcal{T}},t\right)\right\}.\end{aligned} \tag{7}$$

If we choose our filter $\boldsymbol{\mathcal{R}}(q^{-1})$ such that $\mathcal{L}_2(\boldsymbol{\mathcal{R}}^T,\boldsymbol{\mathcal{T}},\lambda) = \mathcal{L}_3(\boldsymbol{\mathcal{T}}^T,\boldsymbol{\mathcal{R}},\lambda) = 0$, then our candidate filter $\boldsymbol{\mathcal{R}}(q^{-1})$ is optimal since $\mathcal{L}_4(\boldsymbol{\mathcal{T}}^T,\boldsymbol{\mathcal{T}},\lambda)$ is quadratic in $\boldsymbol{\mathcal{T}}(q^{-1})$ and thus, no $\boldsymbol{\mathcal{T}}$ can decrease the value of $\mathcal{L}(\boldsymbol{\mathcal{R}}+\boldsymbol{\mathcal{T}},\lambda)$.

The condition $\mathcal{L}_3(\boldsymbol{\mathcal{T}}^T,\boldsymbol{\mathcal{R}},\lambda) = 0$ corresponds to

$$E\left\{\left(\boldsymbol{x}^T\left(\boldsymbol{\mathcal{T}},t\right), \sqrt{\lambda}\boldsymbol{y}^T\left(\boldsymbol{\mathcal{T}},t\right)\right)\begin{pmatrix}\boldsymbol{x}\left(\boldsymbol{\mathcal{R}},t\right)\\ \sqrt{\lambda}\boldsymbol{y}\left(\boldsymbol{\mathcal{R}},t\right)\end{pmatrix}\right\} = 0. \tag{8}$$

In other words, the joint signal vector represented by the $\boldsymbol{x}(t)$ and $\boldsymbol{y}(t)$ generated by our candidate filter $\boldsymbol{\mathcal{R}}(q^{-1})$ should be orthogonal to any additive contributions that could be obtained by admissible perturbations $\boldsymbol{\mathcal{T}}(q^{-1})$ of the filter. This is the well-known orthogonality condition for Wiener filters applied to all signal components that affect (3).

The orthogonality condition can be used constructively by expressing it in the frequency domain, using Parseval's formula. The condition is that $\boldsymbol{\mathcal{R}}(z^{-1})$ should be chosen such that no

poles of the Parsevalian integrand of $\mathcal{L}_3(\boldsymbol{\mathcal{T}}^T, \boldsymbol{\mathcal{R}}, \lambda)$ lie within $|z| \leq 1$, which guarantees that $\mathcal{L}_3(\boldsymbol{\mathcal{T}}^T, \boldsymbol{\mathcal{R}}, \lambda) = 0$. Filter design equations for uniquely specifying $\boldsymbol{\mathcal{R}}(q^{-1})$ can be obtained from this condition, see Example I below and Appendix A-B. The resulting solution will take the form of a spectral factorization, one or several Diophantine equation(s) and a few polynomial matrix multiplications. The solution to the Diophantine equation can be posed as a system of linear equations with the same number of equations as unknowns for a specific set of polynomial matrix degrees, which is in the present case given by the design method, see Appendix A-B. A good overview over the spectral factorization problem may be found in [28]. The resulting filter $\boldsymbol{\mathcal{R}}(q^{-1})$ is causal and stable and it will uniquely minimize (6) for any given $\lambda \geq 0$.

III. Illustrative Examples

The method description above was stripped of details for the sake of generality. Its use will be clarified in a set of examples below, where a few pre-compensation filters for audio applications are derived. The examples below are constructed in order to highlight various aspects of the behaviour of the causal and constrained filters that result from the proposed method and, in some instances, in order to underscore differences to the existing design methods that produce non-causal filters. The investigation is based on an implementation in a real room, corresponding acoustically roughly to a normal living room, see Appendix C. This set-up is chosen so as to stress the implementability of the produced filters and to excite any problems that may be present in a practical implementation that are perhaps easy to overlook in a purely theory based simulation.

A. Example I. LQ Model Matching With Constrained Filter Power

As previously mentioned, the power gain of the resulting filter is an important aspect of audio filter design. In this example, we shall illustrate how the method for deriving causal precompensator filters under the quadratic constraints described in Section II-C can be used to limit the average power gain of the resulting filter.

Utilizing the system description of Section II-B and expressing the rational matrix system model as a pair of polynomial matrices by a right matrix fraction description, $\boldsymbol{\mathcal{H}} = \boldsymbol{B}\boldsymbol{A}^{-1}$ [16, Ch. 6] yields $\boldsymbol{z}(t) = \boldsymbol{B}(q^{-1})\boldsymbol{A}^{-1}(q^{-1})\boldsymbol{\mathcal{R}}(q^{-1})\boldsymbol{r}(t)$.[2] Here, $\boldsymbol{B}(q^{-1})$ is a polynomial matrix of dimension $M|N$ and $\boldsymbol{A}(q^{-1})$ is $N|N$, with $\det(\boldsymbol{A}(z^{-1}))$ having all zeros in $|z| \leq 1$, since $\boldsymbol{\mathcal{H}}(q^{-1})$ is assumed stable.

[2]Consider the simple example

$$\begin{bmatrix} \frac{b_{11_1} + b_{11_2}q^{-1}}{1 + a_{11_2}q^{-1}} & \frac{b_{12_1} + b_{12_2}q^{-1}}{1 + a_{12_2}q^{-1}} \\ \frac{b_{21_1} + b_{21_2}q^{-1}}{1 + a_{11_2}q^{-1}} & \frac{b_{22_1} + b_{22_2}q^{-1}}{1 + a_{12_2}q^{-1}} \end{bmatrix} = \begin{bmatrix} b_{11_1} + b_{11_2}q^{-1} & b_{12_1} + b_{12_2}q^{-1} \\ b_{21_1} + b_{21_2}q^{-1} & b_{22_1} + b_{22_2}q^{-1} \end{bmatrix} \begin{bmatrix} 1 + a_{11_2}q^{-1} & 0 \\ 0 & 1 + a_{12_2}q^{-1} \end{bmatrix}^{-1},$$

which by factorization of any non-common denominator roots can be extended to arbitrary systems.

Our goal is now to find the stable and causal filter $\boldsymbol{\mathcal{R}}(q^{-1})$ that minimizes the reproduction error vector $\boldsymbol{\varepsilon}(t)$ subject to constrained filter power gain,

$$\begin{aligned} \min_{\boldsymbol{\mathcal{R}}} .\quad & J = E\left\{\boldsymbol{\varepsilon}^T(t)\boldsymbol{\varepsilon}(t)\right\} \\ \text{s.t.}\quad & C = E\left\{\boldsymbol{u}^T(t)\boldsymbol{u}(t)\right\} - e_D\,\varrho \leq 0 \\ \leftrightarrow & \\ \min_{\boldsymbol{\mathcal{R}}} .\quad & J = E\left\{\mathrm{tr}\left(\boldsymbol{\varepsilon}(t)\boldsymbol{\varepsilon}^T(t)\right)\right\} \\ \text{s.t.}\quad & C = E\left\{\mathrm{tr}\left(\boldsymbol{u}(t)\boldsymbol{u}^T(t)\right)\right\} - e_D\,\varrho \leq 0. \end{aligned} \tag{9}$$

Here $e_D \geq 0$ is the maximum accepted filter power gain factor and

$$\begin{aligned} \boldsymbol{u}(t) &= \boldsymbol{\mathcal{R}}(q^{-1})\boldsymbol{r}(t), \\ \boldsymbol{\varepsilon}(t) &= \boldsymbol{V}(q^{-1})\left(\boldsymbol{B}(q^{-1})\boldsymbol{A}^{-1}(q^{-1})\boldsymbol{\mathcal{R}}(q^{-1}) - \boldsymbol{D}(q^{-1})\right)\boldsymbol{r}(t), \\ \varrho\mathbf{P} &= E\left\{\boldsymbol{r}(t)\boldsymbol{r}^T(t)\right\}, \end{aligned} \tag{10}$$

so $\boldsymbol{x}(t) = \boldsymbol{\varepsilon}(t)$ and $\boldsymbol{y}(t) = \boldsymbol{u}(t)$ in (2). The problem thus represents a linear quadratic (LQ) model matching or stochastic feed-forward controller design with a constraint on the average power- (or variance) gain of the controller filter. The scaling factor ϱ is introduced to translate the *signal power* constraint into a *filter power gain* constraint. This is done by increasing the constraint value with increasing signal input power, so that only the power gain, for which the filter is responsible, is considered and not the absolute signal power level.

Note that the optimization problem is here always feasible, as choosing $\boldsymbol{\mathcal{R}} = 0$ will always satisfy the constraint.

To solve the problem (9), we formulate the Lagrange objective function (3), which in this case is given by

$$\mathcal{L}(\boldsymbol{\mathcal{R}}, \lambda) = E\left\{\mathrm{tr}\left(\varepsilon(t)\varepsilon^T(t)\right) + \lambda\mathrm{tr}\left(\boldsymbol{u}(t)\boldsymbol{u}^T(t)\right) - \lambda e_D\,\varrho\right\}. \tag{11}$$

The multiplier λ for which optimality of (9) is obtained is found by iteratively changing λ until the value that maximizes (4) is found. The pair $\boldsymbol{\mathcal{R}}_{opt}$, λ_{opt} then constitute the optimal solution to the original optimization problem.

It is shown in Appendix A-B that the filter, $\boldsymbol{\mathcal{R}}$, that minimizes $\mathcal{L}(\boldsymbol{\mathcal{R}}, \lambda)$ for a given value of λ is uniquely given by the expression

$$\boldsymbol{\mathcal{R}}_{opt}(q^{-1}) = \boldsymbol{A}(q^{-1})\boldsymbol{\beta}^{-1}(q^{-1})\boldsymbol{Q}(q^{-1}), \tag{12}$$

where $\boldsymbol{\beta}(q^{-1})$ is a stably and causally invertible $N|N$ polynomial matrix given by the spectral factorization equation

$$\boldsymbol{\beta}_*(q)\boldsymbol{\beta}(q^{-1}) = \boldsymbol{B}_*(q)\boldsymbol{V}_*(q)\boldsymbol{V}(q^{-1})\boldsymbol{B}(q^{-1}) + \lambda\boldsymbol{A}_*(q)\boldsymbol{A}(q^{-1}). \tag{13}$$

The matrix $\boldsymbol{Q}(q^{-1})$ in (12) is an $N|l$ matrix of polynomials which, together with the $N|l$ matrix $\boldsymbol{L}_*(q)$ of non-causal polynomials is given by the unique solution to the Diophantine polynomial matrix equation

$$\boldsymbol{\beta}_*(q)\boldsymbol{Q}(q^{-1}) - \boldsymbol{B}_*(q)\boldsymbol{V}_*(q)\boldsymbol{V}(q^{-1})\boldsymbol{D}(q^{-1}) = q\boldsymbol{L}_*(q). \tag{14}$$

The constraint on $C(\boldsymbol{\mathcal{R}})$ affects the pre-compensation filter expression (12) via $\boldsymbol{\beta}(q^{-1})$, obtained from the spectral factorization (13). Although the constraint is a scalar, it will affect the filter differently in different frequency regions and for different components of $\boldsymbol{u}(t)$. For example, consider the scalar case ($M = N = l = 1$) with an FIR channel $z(t) = \boldsymbol{B}(q^{-1})u(t)$, so $\boldsymbol{A}(q^{-1}) = 1$. By (13), the optimal scalar multiplier λ will then affect the properties of $\boldsymbol{\beta}(e^{-j\omega})$ significantly in frequency regions where the magnitude of λ is significant compared to the power gain $\boldsymbol{B}_*\boldsymbol{V}_*\boldsymbol{V}\boldsymbol{B}$. The constraint will have insignificant effect, as compared to the unconstrained solution ($e_D \rightarrow \infty \Rightarrow \lambda_{opt} \rightarrow 0$) in other frequency regions.

It can be shown that the polynomial matrix spectral factorization equation (13) will have a solution $\boldsymbol{\beta}(q^{-1})$ with stable and causal inverse $\boldsymbol{\beta}^{-1}(q^{-1})$, as required in (12), if and only if the right hand side of (13) has full rank N on the unit circle, when substituting $z = e^{j\omega}$ for q. For this to be true, at least one of the two terms on the right hand side of (13) must have full rank N on $z = e^{j\omega}$, i.e. on $|z| = 1$.

This property cannot be guaranteed in general, so a small additive input penalty regularization may have to be added to the criterion (10), $J = E\{\mathrm{tr}(\boldsymbol{\varepsilon}(t)\boldsymbol{\varepsilon}^T(t)) + \gamma \mathrm{tr}(\boldsymbol{u}(t)\boldsymbol{u}^T(t))\}$, where $\gamma > 0$ is a real-valued scalar. This will result in a third term, $\gamma \boldsymbol{A}_*(q)\boldsymbol{A}(q^{-1})$ on the right hand side of (13). For the (asymptotically) stable systems we investigate here, $\boldsymbol{\mathcal{H}}(q^{-1}) = \boldsymbol{B}(q^{-1})\boldsymbol{A}^{-1}(q^{-1})$, $\det(\boldsymbol{A}(z^{-1}))$ has full rank N on $|z| = 1$, so this term will always guarantee full rank of (13) on $|z| = 1$.

Let us also briefly discuss cases where the other terms may secure full rank, making the regularization superfluous.

First, the term $\lambda \boldsymbol{A}_*(z)\boldsymbol{A}(z^{-1})$ in (13) will have full rank on $|z| = 1$ whenever $\lambda \neq 0$. As discussed in Appendix A-B, $\lambda \neq 0$ whenever the constraint is active. However, the constraint may be inactive, resulting in $\lambda = 0$, so we cannot rely on this term. As an aside, we note that the regularization described above can be interpreted as a lower bound on the addition of the here utilized constraint function to the Lagrange function (11) by $(\lambda + \gamma)E\{\mathrm{tr}(\boldsymbol{u}(t)\boldsymbol{u}^T(t))\}$.

Second, if $\boldsymbol{V}(q^{-1})$ is chosen to have full rank M on $|z| = 1$, then the rank on $|z| = 1$ of the first right hand term of (13), $\boldsymbol{B}_*(z)\boldsymbol{V}_*(z)\boldsymbol{B}(z^{-1})\boldsymbol{V}(z^{-1})$ equals the rank of the $M|N$ system matrix $\boldsymbol{B}(z^{-1})$ on $|z| = 1$. With fewer control points than loudspeaker inputs, $M < N$, we can obviously not have rank N. When $M \gg N$, the risk of $\boldsymbol{B}(z^{-1})$ having rank $< N$ on $|z| = 1$ decreases rapidly with an increasing number of control points M. In all experiments described below, $M = 16$ and $N = 9$ was used, and a regularization was not required.

Finally, we stress again that the case $\lambda = 0$ is only special when the rank of the right hand side of (13) depends on the contribution of the constraint function. This situation must be avoided in order to ensure solvability of the constrained problem.

A filter for 9 loudspeakers generated by the method described above, based on measurements of a room as described in Appendix C, was evaluated by means of transfer function measurement based simulations.

In Fig. 3, we see the spectral properties of this filter. The thick, black line shows the total filter power gain. The power constraint we use states that the average power gain may not exceed -22.5 dB. This choice is made in order to make sure the constraints are invoked and is arrived at in conjunction with the selection of the target bright zone pressure of the target matrix. We choose the desired sound pressure in each design point to be approximately what the system produces with a white unit variance input signal. By choosing filter gains well below 0 dB, being the equivalent gain of the system without filters in line as is the case in the initial measurements, we ensure that the constraints are invoked in the design process. Note, by the overlap of the horizontal dashed lines, that the constraint is attained with equality. This will always be the case provided that the constraint is not satisfied by $\lambda = 0$. The reason for this is that the smallest multiplier λ that leads to constraint satisfaction is optimal, while increasing λ reduces the constraint function value, see Appendix A-A2.

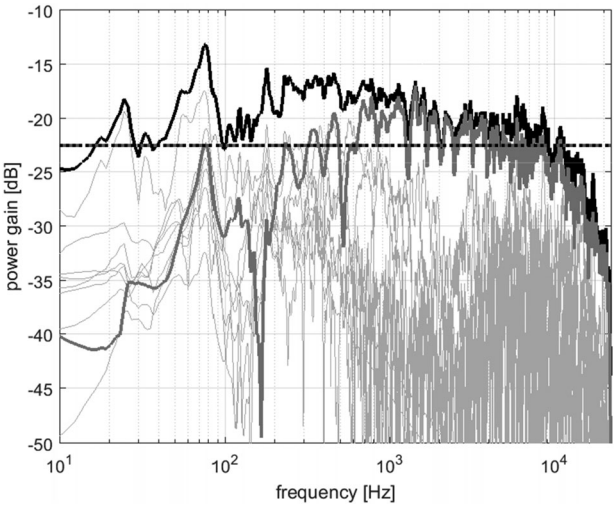

Fig. 3. Power gains of the constrained causal filter described in Section III-A. Total filter power in thick black and each individual filter for 9 loudspeakers in thin gray. The loudspeaker that is directly aligned with the target propagation pattern (loudspeaker six) is represented by the thick gray line. The overlapping horizontal dotted (black) and dash-dotted (gray) lines indicate the achieved mean power gain and the constraint level respectively.

We have here, by (10), constrained the square Euclidian norm of the output $E\{\boldsymbol{u}^T(t)\boldsymbol{u}(t)\} = \sum_{i=1}^{N} |\boldsymbol{u}_i(t)|^2 < e_D \varrho$, relative to the power scaling factor ϱ of the driving noise $r(t)$ while the power distribution over the loudspeakers is free. This means, as is apparent in Fig. 3, that the filter gain typically deviates significantly from the constraint at each frequency. The gray lines show the power spectra of each individual loudspeaker filter. Notably, one such filter (indicated by a thicker line width and darker color) has significantly higher gain than the others at most frequencies. This filter drives loudspeaker six (see Fig. 10), which is directly aligned with the target sound wave propagation by design of $\boldsymbol{D}(q^{-1})$, see Appendix C-A. It makes intuitive sense that the loudspeaker in the best position to recreate the desired sound field is used more than the other loudspeakers that may instead focus on e.g. cancelling reflections.

With a measurement based FIR system representation containing 20000 taps, and a delayed unit impulse target matrix, each of the optimizing pre-compensator elements in this case have 1683 numerator taps and 20000 denominator taps, see Appendix A-B.

B. Example II. Multiple Power Gain Constraints

In the above example, a single constraint was employed for the whole spectral band. This simple formulation may result in a filter with unexpected and perhaps non desired spectral distribution being preferred by the optimization. This is exemplified, at least to some extent, in Fig. 3. We may also wish to constrain several different aspects of the filter simultaneously. It will therefore be beneficial to have a method that allows for multiple constraints. In this example, we derive such a filter by utilizing K power gain constraints instead of one single power gain constraint. Here, each of the K constraints target different frequency regions and/or different components of the control signal vector $\boldsymbol{u}(t)$. Define filtered control signals $\boldsymbol{u}_k(t)$ according to

$$\boldsymbol{u}_k(t) = \boldsymbol{\phi}_k(q^{-1})\boldsymbol{\mathcal{R}}(q^{-1})r(t), \tag{15}$$

where $\boldsymbol{\phi}_k(q^{-1})$ is a monic $N|N$ polynomial matrix with FIR band pass filters for coefficients. The matrix $\boldsymbol{\phi}$ is used to separate the frequency bands and/or loudspeakers for which the mean power gain should be no greater than e_{Dk}. We then use the problem formulation

$$\begin{aligned}\min_{\boldsymbol{\mathcal{R}}}. \quad & J = E\left\{\mathrm{tr}\left(\boldsymbol{\varepsilon}(t)\boldsymbol{\varepsilon}^T(t)\right)\right\} \\ \text{s.t.} \quad & C_1 = E\left\{\mathrm{tr}\left(\boldsymbol{u}_1(t)\boldsymbol{u}_1^T(t)\right)\right\} - e_{D1}\varrho \le 0 \\ & \vdots \\ & C_K = E\left\{\mathrm{tr}\left(\boldsymbol{u}_K(t)\boldsymbol{u}_K^T(t)\right)\right\} - e_{DK}\varrho \le 0. \end{aligned} \tag{16}$$

Above, $\boldsymbol{\varepsilon}(t)$ is defined as in (10). Possible applications of this problem formulation are e.g. to constrain each loudspeaker so that it is active only within a specified frequency interval or to limit the average power gain of each loudspeaker individually. Different loudspeakers are addressed by the different rows of the filter matrix under optimization, $\boldsymbol{\mathcal{R}}(q^{-1})$.

The corresponding Lagrange function can now be defined,

$$\begin{aligned}&\mathcal{L}_{mc}(\boldsymbol{\mathcal{R}}, \lambda_1, \ldots, \lambda_K) \\ &= E\left\{\mathrm{tr}\left(\boldsymbol{\varepsilon}(t)\boldsymbol{\varepsilon}^T(t)\right) + \sum_{k=1}^{K}\lambda_k\left(\mathrm{tr}\left(\boldsymbol{u}_k(t)\boldsymbol{u}_k^T(t)\right) - e_{Dk}\varrho\right)\right\}.\end{aligned} \tag{17}$$

The only difference in the solution as compared to the single power constraint formulation is in the resulting spectral factorization equation that defines the matrix $\boldsymbol{\beta}(q^{-1})$ in (12), which is now given by

$$\boldsymbol{\beta}_*\boldsymbol{\beta} = \boldsymbol{B}_*\boldsymbol{V}_*\boldsymbol{V}\boldsymbol{B} + \sum_{k=1}^{K}\lambda_k\boldsymbol{A}_*\boldsymbol{\phi}_{k*}\boldsymbol{\phi}_k\boldsymbol{A}. \tag{18}$$

The above result is easily obtained by following the proof in A-B but substituting (17) for (11) and (18) for (13)/(40).

Since we now have K constraints, we also have K multipliers λ_k. These represent different dimensions of the now $K-$ dimensional search space, increasing the complexity and therefore the computational time for obtaining the solution.

A filter is now constructed based on this method for the same system as described in Section III-A and Appendix C. The average filter gain is divided into six frequency bands, with associated maximally allowed power gain levels of -22.5 dB. The spectral properties of this filter are shown in Fig. 4. The borders of the frequency bands of the constraints are shown as dashed vertical lines.

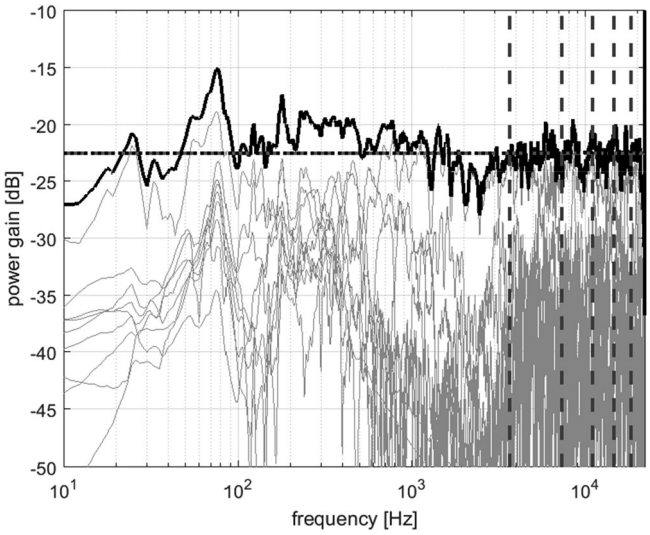

Fig. 4. Power gains of the multiply power constrained causal filter described in Section III-B. Total filter gain in thick black and each individual filter gain in thin gray. Borders of constraint frequency bands are marked by dashed vertical lines. Overlapping horizontal dotted (black) and dash-dotted (gray) lines indicate the attained mean PSD gains and the constraint level respectively.

Compared to the singly power gain constrained filter, Fig. 3, the spectral distribution of the filter power gain is now more even, and the frequency by frequency adherence to the constraint level is increased.

C. High Density Frequency Domain Constraints

It is often motivated to constrain the average over a frequency band but there may arise situations where very detailed control over a large portion of the frequency domain is required.

At a certain point, defining sufficiently many and sufficiently narrow band pass filtering matrices ($\boldsymbol{\phi}_k(q^{-1})$ in (15)) becomes impractical. We will therefore investigate a method for increasing the frequency domain precision of the constraints by using a weighting matrix instead of a large number of band pass filters.

In the non-causal case, outlined in Section III-D below, the constraint function is specified at each center frequency of the spectral design resolution. In the present, causal, context this can be expressed by

$$\begin{aligned}\min_{\boldsymbol{\mathcal{R}}}. \quad & E\left\{\boldsymbol{x}^T(\boldsymbol{\mathcal{R}}, t)\,\boldsymbol{x}(\boldsymbol{\mathcal{R}}, t)\right\} \\ \text{s.t.} \quad & \mathcal{F}\left\{E\left\{\boldsymbol{y}^T(\boldsymbol{\mathcal{R}}, t)\,\boldsymbol{y}(\boldsymbol{\mathcal{R}}, t)\right\}\right\}\Big|_{f_1} - e_1\varrho \le 0 \\ & \vdots \\ \text{s.t.} \quad & \mathcal{F}\left\{E\left\{\boldsymbol{y}^T(\boldsymbol{\mathcal{R}}, t)\,\boldsymbol{y}(\boldsymbol{\mathcal{R}}, t)\right\}\right\}\Big|_{f_K} - e_K\varrho \le 0. \end{aligned} \tag{19}$$

Above, $\mathcal{F}\{\cdot\}|_{f_k}$ denotes the discrete Fourier transform evaluated at frequency f_k.

The Lagrangian associated with (19) becomes

$$\mathcal{L}(\boldsymbol{\mathcal{R}}, \lambda_1, \ldots, \lambda_K) = E\left\{\boldsymbol{x}^T(\boldsymbol{\mathcal{R}}, t)\,\boldsymbol{x}(\boldsymbol{\mathcal{R}}, t)\right\} + \sum_k \lambda_k \mathcal{F}\left\{E\left\{\boldsymbol{y}^T(\boldsymbol{\mathcal{R}}, t)\,\boldsymbol{y}(\boldsymbol{\mathcal{R}}, t)\right\}\right\}\Big|_{f_k} - \sum_k \lambda_k e_k \varrho \tag{20}$$

Introducing an ideal (thus also non-causal), diagonal band pass filter matrix $\boldsymbol{U}_k$ that allows frequency f_k with gain 1 while rejecting all other frequencies, we have

$$\mathcal{L}(\boldsymbol{\mathcal{R}}, \lambda_1, \ldots, \lambda_K) = E\left\{\boldsymbol{x}^T(\boldsymbol{\mathcal{R}}, t)\,\boldsymbol{x}(\boldsymbol{\mathcal{R}}, t)\right\} + \sum_k E\left\{\lambda_k \left(\boldsymbol{U}_k \boldsymbol{y}(\boldsymbol{\mathcal{R}}, t)\right)^T \boldsymbol{U}_k \boldsymbol{y}(\boldsymbol{\mathcal{R}}, t)\right\} - \sum_k \lambda_k e_k \varrho. \tag{21}$$

Since $\boldsymbol{U}_k \boldsymbol{U}_j = 0, \text{ for } k \neq j$, this can be expressed, defining

$$\boldsymbol{U} = \sum_k \sqrt{\lambda_k}\boldsymbol{U}_k, \tag{22}$$

as

$$\mathcal{L}(\boldsymbol{\mathcal{R}}, \boldsymbol{U}) = E\left\{\boldsymbol{x}^T(\boldsymbol{\mathcal{R}}, t)\,\boldsymbol{x}(\boldsymbol{\mathcal{R}}, t)\right\} + E\left\{\left(\boldsymbol{U}\boldsymbol{y}(\boldsymbol{\mathcal{R}}, t)\right)^T \boldsymbol{U}\boldsymbol{y}(\boldsymbol{\mathcal{R}}, t)\right\} - \sum_k \lambda_k e_k \varrho. \tag{23}$$

The minimizing controller $\boldsymbol{\mathcal{R}}(q^{-1})$ is found by setting (c.f. (39), (41) in Appendix A-B)

$$\frac{1}{2\pi j}\oint_{|z|=1} \operatorname{tr}\left[\boldsymbol{x}_*(\boldsymbol{\mathcal{T}}_*, z)\,\boldsymbol{x}\left(\boldsymbol{\mathcal{R}}, z^{-1}\right) + \boldsymbol{y}_*(\boldsymbol{\mathcal{T}}_*, z)\,\boldsymbol{U}_*\left(z, z^{-1}\right)\boldsymbol{U}\left(z, z^{-1}\right)\boldsymbol{y}\left(\boldsymbol{\mathcal{R}}, z^{-1}\right)\right]\frac{dz}{z} = 0. \tag{24}$$

Similarly, using Parsevals' formula, we can write $\mathcal{G}(\lambda)$ as

$$\mathcal{G}(\lambda) = \frac{1}{2\pi j}\oint_{|z|=1} \operatorname{tr}\left[\boldsymbol{x}_*(\boldsymbol{\mathcal{R}}^o_*, z)\,\boldsymbol{x}\left(\boldsymbol{\mathcal{R}}^o, z^{-1}\right) + \boldsymbol{y}_*(\boldsymbol{\mathcal{R}}^o_*, z)\,\boldsymbol{U}_*\left(z, z^{-1}\right)\boldsymbol{U}\left(z, z^{-1}\right)\boldsymbol{y}\left(\boldsymbol{\mathcal{R}}^o, z^{-1}\right)\right]\frac{dz}{z} - \sum_k \lambda_k e_k \varrho \tag{25}$$

where $\boldsymbol{\mathcal{R}}^o$ is the controller that solves (24).

The spectral factorization equation from which the unique minimizer $\boldsymbol{\mathcal{R}}$ can be constructed is found by substituting $\boldsymbol{U}_*\boldsymbol{U}(q, q^{-1})$ for $(\sum_{k=1}^K \lambda_k \boldsymbol{\phi}_{k*}\boldsymbol{\phi}_k)$ in (18), yielding

$$\boldsymbol{\beta}_*\boldsymbol{\beta} = \boldsymbol{B}_*\boldsymbol{V}_*\boldsymbol{V}\boldsymbol{B} + \boldsymbol{A}_*\boldsymbol{U}_*\boldsymbol{U}\boldsymbol{A}. \tag{26}$$

Disregarding the constraints, the use of a weighting matrix to balance the control signal penalty to the target adherence in the objective function corresponds to the method employed in the weighted criterion approach utilized in e.g. [17]–[21].

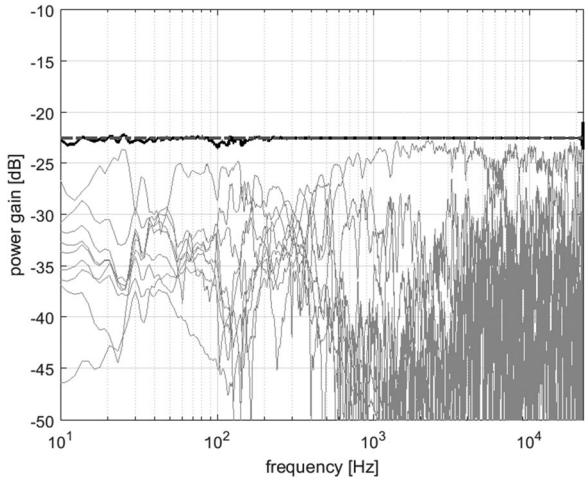

Fig. 5. Power gains of the per-frequency constrained causal filter described in Section III-C. Thick black is total filter power gain and thin gray lines indicates the gains of individual loudspeaker filters. Horizontal dash-dotted (gray) indicates the constraint level.

Note that while we cannot design a set of ideal band pass filters in practice, we *can* manipulate the per-frequency gain of $\boldsymbol{U}_*\boldsymbol{U}$ until we satisfy the primal constraints.

The practical method for maximizing $\mathcal{G}(\lambda)$ will here be to adjust the per-frequency gain of the matrix $\boldsymbol{U}_*\boldsymbol{U}$ at frequency k, which corresponds to adjusting λ_k per (22).

One method for designing the weighting matrix $\boldsymbol{U}_*\boldsymbol{U}$ is to start with an initial guess and iteratively update the frequency domain version of $\boldsymbol{U}_*\boldsymbol{U}$ by $\mathcal{F}\{\boldsymbol{U}_*\boldsymbol{U}\}|_{f_k} \Leftarrow \mathcal{F}\{\boldsymbol{U}_*\boldsymbol{U}\}|_{f_k} \times 10^{step \times err}$, where $err = \mathcal{F}\{E\{\boldsymbol{y}^T\boldsymbol{y}\}\}|_{f_k} - e_k\varrho$ and $step$ is a step length. This method will reduce the per-frequency gain of $\boldsymbol{U}_*\boldsymbol{U}$ where there is room in the constraint and increase the gain where the constraint is not satisfied. Note that the convergence of this algorithm cannot be guaranteed, as interdependence between the gains at different frequencies is not accounted for. This has not been a problem in the practical filter computations in the example presented in the current paper, probably due to the frequency domain smoothness of the utilized constraint values. A safer route is to use an existing, tried, convex optimization algorithm to find $\boldsymbol{U}_*\boldsymbol{U}$.

The power spectrum of the resulting causal per-frequency constrained filter is shown in Fig. 5, using 8038 per-frequency power constraints. The constraint of -22.5 dB is fulfilled to the tolerance of the search algorithm but with more variability at lower frequencies. Compared to the two filters previously described in Sections III-A and III-B, the present constraint is considerably more strict, c.f. Figs. 3 and 4.

D. The Corresponding Frequency-Domain Design

A general method for finding the frequency domain non-causal filter counterparts to the equations presented above is described in [5, Appendix B]. The method utilized here will produce an FIR filter, and so care must be taken that the produced filters are sufficiently long that any ill effects of truncation are kept at a minimum. The version outlined below corresponds to the case with constrained filter power spectral density gains.

The frequency domain representation of the system described in Section II-B is here utilized. The system matrix at angular frequency ω_i is therefore $\mathbf{H}_i = \boldsymbol{\mathcal{H}}(e^{-j\omega_i})$. All other matrices follow the same pattern. We define the problem at frequency ω_i as

$$\begin{aligned} \min_{\mathbf{R}_i} . \quad & J_i = ||\mathbf{V}_i \left(\mathbf{H}_i\mathbf{R}_i - \mathbf{D}_i\right)||_2^2 \\ \text{s.t.} \quad & C_i = ||\mathbf{R}_i||_2^2 - e_{D\,i} \leq 0, \end{aligned} \tag{27}$$

for a scalar driving noise ($l = 1$). The dimensions of the above complex-valued constant matrices are, at each frequency bin, the same as the corresponding polynomial matrices. Thus $\dim(\mathbf{R}_i) = N|1$, $\dim(\mathbf{H}_i) = M|N$, $\dim(\mathbf{V}_i) = M|M$, $\dim(\mathbf{D}_i) = M|1$.

This problem can be solved for each frequency bin of the discrete Fourier domain representation of the original system by separating the real and imaginary parts and stacking them, generating a convex problem. When a solution for each frequency bin has been obtained, the total complex filter matrix $\mathbf{R}_{tot}$ is assembled, and inverse transformed if the filtering is to be executed in time domain.

The problem (27) is solved by computing the compensation matrix at frequency ω_i by solving the vectorized real valued problem

$$\mathbf{R}_i = \left(\mathbf{M}_R^T + \lambda_i\mathbf{I}\right)^{-1}\mathbf{M}_D, \tag{28}$$

where

$$\begin{aligned} \mathbf{M}_D &= \begin{bmatrix} \mathrm{Re}\left(\mathbf{H}^H\mathbf{V}^H\mathbf{V}\mathbf{D}\right) \\ \mathrm{Im}\left(\mathbf{H}^H\mathbf{V}^H\mathbf{V}\mathbf{D}\right) \end{bmatrix} \\ \mathbf{M}_R &= \begin{bmatrix} \mathrm{Re}\left(\mathbf{H}^H\mathbf{V}^H\mathbf{V}\mathbf{H}\right) & -\mathrm{Im}\left(\mathbf{H}^H\mathbf{V}^H\mathbf{V}\mathbf{H}\right) \\ \mathrm{Im}\left(\mathbf{H}^H\mathbf{V}^H\mathbf{V}\mathbf{H}\right) & \mathrm{Re}\left(\mathbf{H}^H\mathbf{V}^H\mathbf{V}\mathbf{H}\right) \end{bmatrix}, \end{aligned} \tag{29}$$

See Appendix B. Above, λ_i is found by solving the concave linear matrix inequality optimization problem

$$\begin{aligned} \max . \quad & \gamma_i \\ \text{s.t.} \quad & \lambda_i \geq 0 \\ & \begin{bmatrix} \mathbf{M}_R^T + \lambda_i\mathbf{I} & \mathbf{M}_D \\ \mathbf{M}_D^T & -\lambda_i e_{D\,i} - \gamma_i \end{bmatrix} \succeq 0. \end{aligned} \tag{30}$$

Implementing this filter in the model system, using an FIR filter length of 16077 taps, yields the power distribution shown in Fig. 6. The average power gain of the filter shows little deviation from the target curve and the deviation that is present is not that surprising, as it is a numerical method that requires a matrix inversion in order to find the filter.

A causal IIR filter solution of (27) can be constructed using the method described in III-C.

Comparing Figs. 6 to 5, the non-causal filters shown in Fig. 6 display much greater variations in power gains for individual loudspeakers. In the causally constrained filter, a single loudspeaker is dominant for the majority of frequencies. This indicates an important robustness issue in the causally unconstrained design, where phase (or frequency) drift between the loudspeaker filters would have more severe effects than in the causally constrained case. This situation could e.g. arise where the clocks of the different digital filter outputs are not properly synchronized. This behaviour may also lead to issues e.g. in cases where the loudspeaker models are imperfect, e.g. due to manufacturing variations or temperature related loudspeaker phase response variations.

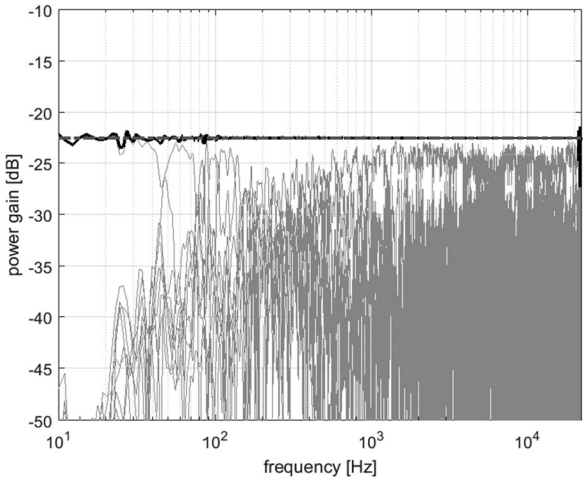

Fig. 6. Power gains of the per-frequency constrained filter without constraints on causality described in Section III-D. Thick black is total filter power gain and thin gray lines indicate the gains of individual loudspeaker filters. Horizontal dash-dotted (gray) indicates the constraint level.

E. Target Reproduction

The objective of all designs investigated here is to minimize the difference between the resulting compensated system output and a target sound field, specified in the $M|l$ FIR filter matrix $\boldsymbol{D}$. The largest difference between the novel causally constrained filter and the frequency domain formulated filter is expected to be evident in the target reproduction properties. The adherence to the desired system behaviour of the system as compensated by the causally unconstrained frequency domain formulated filter described in Section III-D is therefore compared to that of a causal per-frequency constrained design found by the method of Section III-C. Both filters are thus constrained similarly at each frequency but one is computed with a constraint on filter causality, whereas the other is not.

The simulated average power spectral density of the electro-acoustical system at the control points, compensated with the two filters resulting from the design methods specified above, $\boldsymbol{\mathcal{HR}}$, is shown in Fig. 7 along with the power spectral density of the target vector $\boldsymbol{D}(q^{-1})$. The target gain is chosen large enough that the filter power gain constraints would need to be violated in order to achieve perfect reconstruction, therefore the target can not be attained for all frequencies. This is a concious design choice since a design that does not invoke the constraints is no different from a design without constraints.

The causally unconstrained filter attains a better target reproduction, spectrally speaking, than the constrained filter does. This is not a very surprising result, as adding constraints (in this case on causality) cannot improve the criterion value. The advantage of the non-causal method is more pronounced at the lower frequencies whereas the methods seem more equal for

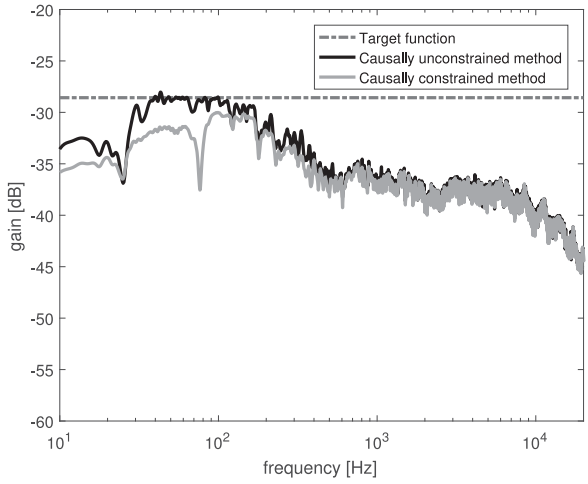

Fig. 7. Average frequency response of compensated system for both the causally constrained and unconstrained filters. Dot-dashed line shows the target function gain, gray and black represent the causally unconstrained method and the causally constrained method respectively.

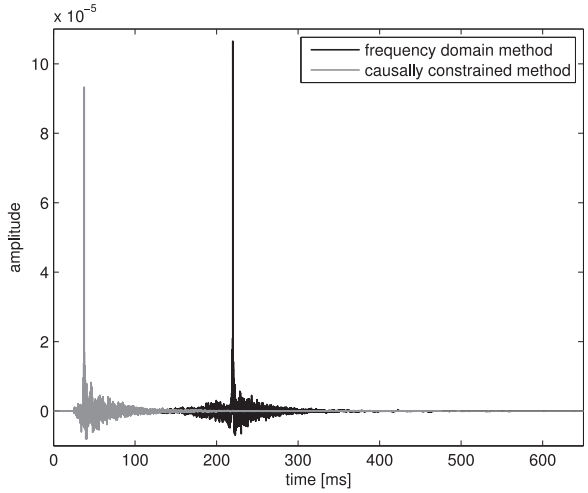

Fig. 8. Taps of the impulse response of the compensated system to one control point when using the causally constrained filter (gray) and the causally unconstrained filter (black). The impulse responses are truncated after 650 ms in order to improve readability.

frequencies above (roughly) 500 Hz. The effect that the influence of causality is concentrated to the lower frequencies is in agreement with previous findings [19].

Comparing the time-domain behaviour of the two methods is more complicated than the frequency domain ditto since the main peaks of the impulse responses of the two compensated systems do not match in time. This is in turn due to the non-causal nature of the frequency domain formulated filter. The impulse responses of the compensated systems are shown in Fig. 8 at a control point in the middle of the grid.

A notable difference, aside from the timing of the filter action, is the time during which pre-ringings are present in the compensated impulse response. Quantifying the audibility of the pre-ringings is not very straight forward but previous studies indicate that the effect of auditory pre-masking is only reliable up to 20 ms before the main impulse [1]. This implies that the

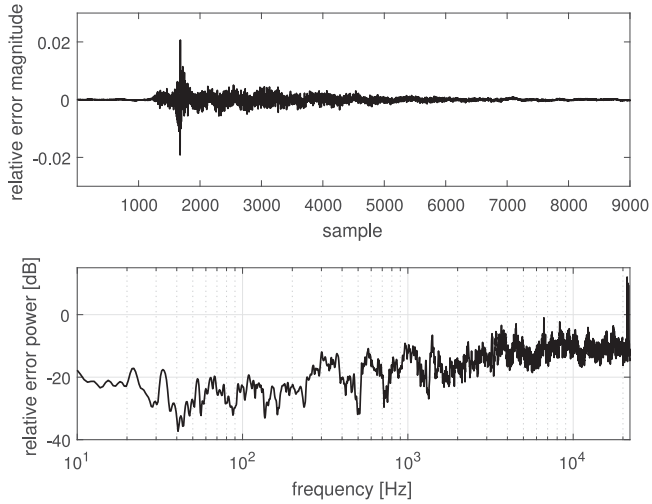

Fig. 9. Accuracy of simulated compensated transfer functions. Sample-by-sample average simulation error relative to the largest simulated sample. Top figure: Time domain. Bottom figure: Frequency domain.

temporal properties of the causally unconstrained filter will be more problematic from a psychoacoustics point of view. This drawback in the time domain may be compensated for by the better target adherence in the frequency domain (see Fig. 7) but practical experience indicates that the temporal aspects play an important role, at least when it comes to high fidelity audio.

The misalignment in time of the main impulse of the causally unconstrained filter relative to the target impulse obviously generates a large temporal reconstruction error. This could be rectified by simply truncating the filter, but that would cause significant additional errors in the frequency domain instead. Another method is to cyclically shift the time domain taps of the filter, but this typically generates a non-negligible post-echo in the compensated impulse response. A compromise of the two can be achieved by shifting the filter taps and windowing the frequency domain representation of the filter [29, Appendix C]. These are however post-optimization fixes and do not guarantee an optimal filter, as the causally constrained methods do.

F. Filter Validity

Theoretical filter design is of little use if the produced filters generate nonsensical or undesired output. In order to verify that this is not the case with the present filters, an experiment is performed to compare the simulations to real experimental results. The same singly constrained filter described in Section III-A is used for both the simulations and the validation measurements. Differences of the compensated system response between the simulation and a real life measurement should therefore reveal the effect of any model errors. The difference between the simulated responses and validation measurements using the same pre-compensation filter is shown in Fig. 9.

The errors shown are averaged over all measurement positions and are shown in both time and frequency domain. In order not to average out the larger errors in the main peak, the measurements have been time aligned so that the delays of the main peaks of the impulse responses in all measurement posi-

tions are the same. The same time shift that was used for the validation measurements is then applied to the simulated impulse responses. The errors shown in Fig. 9 (top) are relative to the maximum peak of the simulated impulse responses. A relative error of 1 would mean that the average error at the corresponding delay (relative to the main peak of the impulse response) is of the same magnitude as the largest main peak of all simulated impulse responses. In the lower, frequency domain figure, the average error power relative to the average power of the simulated system per frequency is shown. This means that a gain of 0 dB indicates that the error power is on average the same as the power of the simulated compensated system at that frequency.

As the filter in question is derived under a single constraint covering the entire frequency band, loudspeakers may be active in frequency bands for which they are not designed. There are however no clear indications that this is the case in the present investigation. We note a large error at the highest end of the spectrum of Fig. 9, but further investigations reveal that the source is background noise in the laboratory environment. In the top figure, we see that the maximum relative error is about two orders of magnitude smaller than the highest peak of the simulated response. As we here look at the compensated system response, as opposed to filter power gain, there may be large modelling errors above 1200 Hz, see Appendix C. The validation measurement positions were approximately the same as the design points, but some spatial deviations are to be expected, thus the error above 1200 Hz may be influenced by over-fitting to the design points. The problem of over-fitting should increase with frequency, as diminishing wavelengths increase the relative error of small deviations and such a trend, albeit weak, is indeed discernible in the validation measurement.

G. Computational Complexity, a Comparison to FIR Matrix Solutions

The causal rational matrix approach that is utilized herein provides control over both the pre-ringing and the delay of the compensated system, as illustrated in Section III-E. Causal (FIR) filters subject to quadratic constraints can also, however, be computed using Toeplitz matrix system descriptions. The main issue in designing filters using the Toeplitz approach is memory constraints, which relate to the length of the filters computed.

The resolving filter of a Toeplitz structured optimization will be of length NI, where N, as above, represents the number of loudspeakers and I the number of filter taps and will typically be structured as a column vector with all taps related to one loudspeaker stacked on top of each other. We here assume that all loudspeakers are driven by filters of the same length, which is a simplification but not one that significantly alters the conclusions.

The direct solution to the Toeplitz matrix optimization of the problems exemplified herein will be structured according to $\mathbf{R} = \mathbf{X}^{-1}\mathbf{Y}$ where $\mathbf{X}$ is a square matrix and $\mathbf{Y}$ is post multiplied with a column vector representing the desired system behaviour. This, by the known dimension of the filter vector $\mathbf{R}$, implies that the matrix $\mathbf{X}$ must be of dimension $NI|NI$. There are methods that avoid the inversion step (e.g. using the Schur complement, see e.g., [30]) but the problem of the size of the matrix central to the solution remains.

Comparing IIR filters to FIR filters in terms of filter length is challenging but the filters produced in Section III herein may be reasonably well approximated by FIR filters of 16000 taps. For a system of 9 loudspeakers and in 64 bit (8 Byte) precision, the matrix to-be-inverted thus requires $(16000 \times 9)^2 \times 8 \approx 166$ GB of memory to be stored. Even if we halve both the numerical precision and the number of taps of the filters, we end up with a $(8000 \times 9)^2 \times 4 \approx 21$ GB matrix to invert which will strain most computers.

Conversely, the spectral factorization equation to be solved for the rational matrix solutions of the examples discussed herein requires $N|N$ elements of FIR filters with (at most) 40001 taps. This follows from how the matrix $\boldsymbol{\beta}_*(q)\boldsymbol{\beta}(q^{-1})$ is constructed, see (40) and that the system matrix is here modelled as a polynomial matrix with degree 19999, see Appendix C. The matrix to-be-spectrally-factored is thus stored using $9 \times 9 \times 40001 \times 8 \approx 26$ MB of memory. Formulating the Diophantine equation by a system of linear equations, this matrix here attains a dimension of $21682|21682$ elements. In 64 bit precision, this requires approximately 3.8 GB of storage memory. This matrix is however largely comprised of blocks of zeros and unit matrices. Disregarding (some of) these blocks, which may be accounted for in other more memory efficient ways, the remaining block is of dimension $21682|1683$ elements with an approximative memory footprint of 292 MB.

The relative computational time of the methods depends on multiple factors. The most important are believed to be, in no particular order, the choice of spectral factorization algorithm, the system size and required length of parametrization and the technique used to find the approximate inverse to the Toeplitz system matrix. For systems with a large amount of loudspeaker channels and long decay times that require a substantial number of FIR filter taps to adequately model and compensate however, the proposed approach is the only computationally viable method of the two.

H. Limitations

There are some limitations of the proposed method. These may be split into two groups, the first of which are user-induced limitations and the second of which are inherent limitations. In the first group we find

- unattainable constraints,
- conflicting constraints and
- allowing too much freedom in the spectral domain

where the last point is perhaps the least self explanatory. The behaviour of the singly constrained filter investigated in Section III-A may be an example where the method is given too much freedom in the frequency domain. The problem being that the filter may behave in a non-desired way for some frequencies so long as the average behaviour satisfies the constraint. All the above limitations are limitations not in the method itself but rather in the utilization of the method.

The second group of limitations is smaller but more fundamental. The primary limitation here is that the spectral factorization equation requires a valid spectrum in order to be successfully solved. This means that the right-hand side of equation (13) must be positive definite at all frequencies on the unit circle $e^{j\omega}$. This can be assured by defining a filter power penalty term in the objective function, so that $J = E\{\boldsymbol{\varepsilon}^T(t)\boldsymbol{\varepsilon}(t) + \boldsymbol{u}^T(t)\boldsymbol{u}(t)\}$ where $\boldsymbol{u}(t) = \boldsymbol{W}(q^{-1})\boldsymbol{\mathcal{R}}(q^{-1})\boldsymbol{r}(t)$ and $\boldsymbol{W}(q^{-1})$ is a penalty matrix that is positive definite for all frequencies. This issue was discussed at greater depth in Section III-A.

IV. Conclusion

The design method presented and exemplified herein extends the current knowledge of causal rational matrix Wiener filter and feedforward regulator design to also include quadratic, variance constraints. This is often useful when the square Euclidian norm of some property influenced by the filter cannot, or should not, exceed a pre-specified limit. The method also extends to include several constraints. A design method for problems with a vast amount of constraints, corresponding to the non-causal per-frequency constrained designs, is also proposed and investigated. The resulting filters from a set of examples have been investigated by simulations and have been shown to behave in a reasonable way. A simulation has also been compared to real life measurements of compensated acoustic transfer functions, with small deviations between the simulation and the measurements. The causality constraint of the design method allows for the designer to reduce pre-ringings of the resulting pre-compensation filters. The causal filter with per-frequency constraints also shows improved robustness with respect to inter-channel frequency drift as opposed to the non-causal filter. This behaviour should be further investigated.

A polynomial approach to discrete-time LQ feedforward compensator design is used in this paper, but the problem can equivalently be posed, and solved, in a state-space setting.

A natural extension to this work is to incorporate the explicit time-domain pre-ringing constraints of [31] and [32] into the design method. The properties of transfer functions in between measurement points can also be taken into account in a statistical sense with methods outlined in [32], [33]. This can be used to increase the robustness of the design and to reduce over-adjustment to the properties of the sound field at the control points.

Appendix A
Derivations of Design Equations

A. Proof of Dual Optimality

We here prove that the dual optimization problem also provides the solution to the primal optimization problem.

We will first show that a controller that minimizes the Lagrange function while providing a certain constraint value also is optimal w.r.t. the constrained optimization problem for the same constraint value. We will then move on to show that the value of the constraint function $C(\boldsymbol{\mathcal{R}})$ decreases monotonically with increasing values for the multiplier λ. We will then show that increasing λ also increases the objective value $J(\boldsymbol{\mathcal{R}})$ monotonically. If the above is true, then the optimal $\boldsymbol{\mathcal{R}}(q^{-1})$ must be found as the minimizer to (3), with λ being the smallest value that results in constraint satisfaction. The Lagrangian (3) is here generalized to multiple constraints as in (17) and (21).

1) A Minimizing Unconstrained Lagrange Controller that Satisfies the Constraints is Optimal for the Constrained Problem: The controller $\boldsymbol{\mathcal{R}}(q^{-1})$ that minimizes $\mathcal{L}(\boldsymbol{\mathcal{R}}, \lambda_1, \ldots, \lambda_K)$ w.r.t. $\boldsymbol{\mathcal{R}}(q^{-1})$ while fulfilling $C_k(\boldsymbol{\mathcal{R}}) = e_k$ with equality will also be an optimal solution to (2) subject to $C_k(\boldsymbol{\mathcal{R}}) = e_k$. If this were not true, we could find a controller $\boldsymbol{\mathcal{S}}(q^{-1})$ for which $J(\boldsymbol{\mathcal{S}}) < J(\boldsymbol{\mathcal{R}})$ while $C_k(\boldsymbol{\mathcal{S}}) = C_k(\boldsymbol{\mathcal{R}}) = e_k$. But then, by (3),

$$\begin{aligned}
&\mathcal{L}(\boldsymbol{\mathcal{R}}, \lambda_1, \ldots, \lambda_K) \\
&> E\left\{\boldsymbol{x}^T(\boldsymbol{\mathcal{S}}, t)\,\boldsymbol{x}(\boldsymbol{\mathcal{S}}, t) + \sum_{k=1}^{K} \lambda_k \left(\boldsymbol{y}_k^T(\boldsymbol{\mathcal{R}}, t)\,\boldsymbol{y}_k(\boldsymbol{\mathcal{R}}, t) - e_k\right)\right\} \\
&= E\left\{\boldsymbol{x}^T(\boldsymbol{\mathcal{S}}, t)\,\boldsymbol{x}(\boldsymbol{\mathcal{S}}, t) + \sum_{k=1}^{K} \lambda_k \left(\boldsymbol{y}_k^T(\boldsymbol{\mathcal{S}}, t)\,\boldsymbol{y}_k(\boldsymbol{\mathcal{S}}, t) - e_k\right)\right\} \\
&= \mathcal{L}(\boldsymbol{\mathcal{S}}, \lambda_1, \ldots, \lambda_K), \qquad (31)
\end{aligned}$$

which contradicts the assumption that $\boldsymbol{\mathcal{R}}(q^{-1})$ minimizes $\mathcal{L}(\boldsymbol{\mathcal{R}}, \lambda_1, \ldots, \lambda_K)$.

2) Increasing λ_k Must Reduce $C_k(\boldsymbol{\mathcal{R}})$: Assume, with no loss of generality, that $\lambda_1 = \lambda_a = a\eta,\ a \in \mathbb{N},\ \eta > 0$. Now, note that if $\boldsymbol{\mathcal{R}}_a$ is the minimizer of $\mathcal{L}(\boldsymbol{\mathcal{R}}, \lambda_a, \lambda_2, \ldots, \lambda_K)$ and $\boldsymbol{\mathcal{R}}_{a+1}$ the minimizer of $\mathcal{L}(\boldsymbol{\mathcal{R}}, \lambda_{a+1}, \lambda_2, \ldots, \lambda_K)$ then $\mathcal{L}(\boldsymbol{\mathcal{R}}_{a+1}, a\eta, \lambda_2, \ldots, \lambda_K) \geq \mathcal{L}(\boldsymbol{\mathcal{R}}_a, a\eta, \lambda_2, \ldots, \lambda_K)$ and $\mathcal{L}(\boldsymbol{\mathcal{R}}_a, (a+1)\eta, \lambda_2, \ldots, \lambda_K) \geq \mathcal{L}(\boldsymbol{\mathcal{R}}_{a+1}, (a+1)\eta, \lambda_2, \ldots, \lambda_K)$, thus

$$\begin{aligned}
&\mathcal{L}(\boldsymbol{\mathcal{R}}_a, (a+1)\eta, \lambda_2, \ldots, \lambda_K) \\
&= \mathcal{L}(\boldsymbol{\mathcal{R}}_a, a\eta, \lambda_2, \ldots, \lambda_K) + \eta C_1(\boldsymbol{\mathcal{R}}_a) \\
&\geq \mathcal{L}(\boldsymbol{\mathcal{R}}_{a+1}, (a+1)\eta, \lambda_2, \ldots, \lambda_K) \\
&= \mathcal{L}(\boldsymbol{\mathcal{R}}_{a+1}, a\eta, \lambda_2, \ldots, \lambda_K) + \eta C_1(\boldsymbol{\mathcal{R}}_{a+1}). \qquad (32)
\end{aligned}$$

Since $\mathcal{L}(\boldsymbol{\mathcal{R}}_{a+1}, a\eta, \lambda_2, \ldots, \lambda_K) \geq \mathcal{L}(\boldsymbol{\mathcal{R}}_a, a\eta, \lambda_2, \ldots, \lambda_K)$, we have

$$C_1(\boldsymbol{\mathcal{R}}_{a+1}) \leq C_1(\boldsymbol{\mathcal{R}}_a). \qquad (33)$$

Letting $\eta \to 0$, and capitalizing on the fact that the order and numbering of the constraint functions is arbitrary, we see that $C_k(\boldsymbol{\mathcal{R}})$ decreases monotonically with increasing λ_k, for any $k = 1, \ldots, K$.

3) The Smallest Values λ_k that Satisfy the Constraints are Optimal: Assume that we have a set of multipliers $\lambda_1, \ldots, \lambda_K$, that leads to the controller $\boldsymbol{\mathcal{R}}_a$ when the function $\mathcal{L}(\boldsymbol{\mathcal{R}}, \lambda_1, \ldots, \lambda_K)$ is minimized. Assume that the controller $\boldsymbol{\mathcal{R}}_a$ has the property that $\lambda_1 C_1(\boldsymbol{\mathcal{R}}_a) = \cdots = \lambda_K C_K(\boldsymbol{\mathcal{R}}_a) = 0$ while $C_k \leq 0$ for $k = 1, \ldots, K$. Let us further assume that the values of the multipliers λ_k are the smallest possible values that achieve an $\boldsymbol{\mathcal{R}}$ with the above properties.

The controller $\boldsymbol{\mathcal{R}}_{a+1}$ is now defined as the minimizer to the function $\mathcal{L}(\boldsymbol{\mathcal{R}}, \lambda_1, \ldots, \lambda_{K-1}, \lambda_K + \eta)$. It constitutes a valid

solution to the primal optimization problem, thus $C_k(\boldsymbol{\mathcal{R}}_{a+1}) \leq 0$ for $k = 1, \ldots, K$.

We also know that

$$\begin{aligned} J(\boldsymbol{\mathcal{R}}_a) + \sum_{k=1}^{K} \lambda_k C_k(\boldsymbol{\mathcal{R}}_a) &= \mathcal{L}(\boldsymbol{\mathcal{R}}_a, \lambda_1, \ldots, \lambda_K) \\ &\leq \mathcal{L}(\boldsymbol{\mathcal{R}}_{a+1}, \lambda_1, \ldots, \lambda_K) = J(\boldsymbol{\mathcal{R}}_{a+1}) + \sum_{k=1}^{K} \lambda_k C_k(\boldsymbol{\mathcal{R}}_{a+1}) \\ &\Rightarrow J(\boldsymbol{\mathcal{R}}_{a+1}) \geq J(\boldsymbol{\mathcal{R}}_a) + \sum_{k=1}^{K} \lambda_k \left(C_k(\boldsymbol{\mathcal{R}}_a) - C_k(\boldsymbol{\mathcal{R}}_{a+1}) \right) \\ &= J(\boldsymbol{\mathcal{R}}_a) + \gamma^2. \end{aligned} \tag{34}$$

Above, γ^2 indicates a non-negative number since increasing any constraint function value would, by the assumption that $\boldsymbol{\mathcal{R}}_a$ provides $\lambda_k C_k(\boldsymbol{\mathcal{R}}) = 0$, violate the corresponding constraint. In the case where $\lambda_k = 0$ provides $C_k(\boldsymbol{\mathcal{R}}) < 0$, the choice of $\lambda_k = 0$ ensures that $\lambda_k C_k(\boldsymbol{\mathcal{R}}_a) - \lambda_k C_k(\boldsymbol{\mathcal{R}}_{a+1}) \geq 0$.

This means that we cannot find a valid solution to the primal optimization problem that provides a smaller primal objective function value than that which achieves $\lambda_k C_k(\boldsymbol{\mathcal{R}}) = 0$, with λ_k assuming the smallest value that provides the above equality through the minimization of the Lagrange function. This optimizing set of multipliers $\lambda_1, \ldots, \lambda_K$ is the set that is found by maximizing (4), as we will show below.

4) Maximizing the Dual Function (4) Provides the Optimal Value λ: Examining the multiply constrained (subjected to multiple constraints) version of (3), particularly in relation to the sign of the last term,

$$\begin{aligned} \mathcal{G}(\lambda) = \min_{\boldsymbol{\mathcal{R}}} E \Bigg\{ & \boldsymbol{x}^T(\boldsymbol{\mathcal{R}}, t)\, \boldsymbol{x}(\boldsymbol{\mathcal{R}}, t) \\ & + \sum_{k=1}^{K-1} \lambda_k \left(\boldsymbol{y}_k^T(\boldsymbol{\mathcal{R}}, t)\, \boldsymbol{y}_k(\boldsymbol{\mathcal{R}}, t) - e_k \right) \\ & + \lambda_K \left(\boldsymbol{y}_K^T(\boldsymbol{\mathcal{R}}, t)\, \boldsymbol{y}_K(\boldsymbol{\mathcal{R}}, t) - e_K \right) \Bigg\}, \end{aligned} \tag{35}$$

we note that given a λ_K that results in $\boldsymbol{y}_K^T(\boldsymbol{\mathcal{R}}, t)\boldsymbol{y}_K(\boldsymbol{\mathcal{R}}, t) > e_K$ (an under-fulfilled constraint), a smaller λ_K must produce a smaller value of $\mathcal{G}(\lambda)$ since reducing λ_K but not altering $\boldsymbol{\mathcal{R}}$ does produce a smaller value of $\mathcal{L}(\boldsymbol{\mathcal{R}}, \lambda)$, and $\mathcal{G}(\lambda)$ assumes the smallest possible value of $\mathcal{L}(\boldsymbol{\mathcal{R}}, \lambda)$ for any $\boldsymbol{\mathcal{R}}$. Likewise, given a λ_K for which $\boldsymbol{y}_K^T(\boldsymbol{\mathcal{R}}, t)\boldsymbol{y}_K(\boldsymbol{\mathcal{R}}, t) < e_K$ (an over-fulfilled constraint), the value of $\mathcal{G}(\lambda)$ must decrease with increasing λ_K. The smallest value of λ_K for which constraint satisfaction is attained ($\lambda_K = 0$ or $C_K(\boldsymbol{\mathcal{R}}) = e_K$) is therefore the same as the maximizing argument of $\mathcal{G}(\lambda)$. Since the constraint order is arbitrary, the same result holds if we swap $C_K = C_k$ for any $k = 1, \ldots, K$, and the result is thus valid for all constraints individually. ■

To summarize, we have shown that the solution to the dual problem, $\max_\lambda . \mathcal{G}(\lambda)$, also optimally solves the primal problem (2). This means that the duality gap is indeed zero for the problem at hand.

B. Derivations of Design Equations (12)–(14) in Section III-A Using Orthogonality in the Frequency Domain

To find the pre-compensation filter $\boldsymbol{\mathcal{R}}$ by (10) that minimizes the extended objective function $\mathcal{L}(\boldsymbol{\mathcal{R}}, \lambda)$ by (11), we will use the variational argument outlined in Section II-C and described in e.g. [24]. The argument is that if we add a term to our controller and then design the composite controller so that our Lagrange function is minimized only if the added term is zero, then our controller will be optimal. In the following, the dependence of the Lagrange function will be omitted in order to keep the equations more succinct. $\mathcal{L}$ should however always be interpreted as $\mathcal{L}(\boldsymbol{\mathcal{S}}, \lambda)$, where $\boldsymbol{\mathcal{S}}$ is a generic filter which may be substituted for $\boldsymbol{\mathcal{R}}, \boldsymbol{\mathcal{R}} + \boldsymbol{\mathcal{T}}$ or $\boldsymbol{\mathcal{T}}$ where relevant.

Starting with the Lagrange function, (11), we add to the controller $\boldsymbol{\mathcal{R}}(q^{-1})$ a causal and stable variation filter $\boldsymbol{\mathcal{T}}(q^{-1})$. Substituting $\boldsymbol{\mathcal{R}} + \boldsymbol{\mathcal{T}}$ for $\boldsymbol{\mathcal{R}}$, we have

$$\begin{aligned} \bar{\boldsymbol{u}}(t) &= \boldsymbol{u}(t) + \boldsymbol{u}'(t) = \boldsymbol{\mathcal{R}}\boldsymbol{r}(t) + \boldsymbol{\mathcal{T}}\boldsymbol{r}(t), \\ \bar{\boldsymbol{\varepsilon}}(t) &= \boldsymbol{\varepsilon}(t) + \boldsymbol{\varepsilon}'(t) \\ &= \boldsymbol{V}\left(\boldsymbol{B}\boldsymbol{A}^{-1}\boldsymbol{\mathcal{R}} - \boldsymbol{D}\right)\boldsymbol{r}(t) + \boldsymbol{V}\boldsymbol{B}\boldsymbol{A}^{-1}\boldsymbol{\mathcal{T}}\boldsymbol{r}(t). \end{aligned} \tag{36}$$

So the function to be minimized is now

$$\mathcal{L} = E\left\{ \mathrm{tr}\left(\bar{\boldsymbol{\varepsilon}}(t)\bar{\boldsymbol{\varepsilon}}^T(t)\right) + \lambda \mathrm{tr}\left(\bar{\boldsymbol{u}}(t)\bar{\boldsymbol{u}}^T(t)\right) - \lambda e_D \varrho \right\}, \tag{37}$$

and can be organized into the four terms (7):

$$\begin{aligned} \mathcal{L} &= \mathcal{L}_1 + \mathcal{L}_2 + \mathcal{L}_3 + \mathcal{L}_4 \\ \mathcal{L}_1 &= E\left\{ \mathrm{tr}\left(\boldsymbol{\varepsilon}(t)\boldsymbol{\varepsilon}^T(t)\right) + \lambda \mathrm{tr}\left(\boldsymbol{u}(t)\boldsymbol{u}^T(t)\right) - \lambda e_D \varrho \right\}, \\ \mathcal{L}_2 &= E\left\{ \mathrm{tr}\left(\boldsymbol{\varepsilon}'(t)\boldsymbol{\varepsilon}^T(t)\right) + \lambda \mathrm{tr}\left(\boldsymbol{u}'(t)\boldsymbol{u}^T(t)\right) \right\}, \\ \mathcal{L}_3 &= E\left\{ \mathrm{tr}\left(\boldsymbol{\varepsilon}(t)\boldsymbol{\varepsilon}'^T(t)\right) + \lambda \mathrm{tr}\left(\boldsymbol{u}(t)\boldsymbol{u}'^T(t)\right) \right\}, \\ \mathcal{L}_4 &= E\left\{ \mathrm{tr}\left(\boldsymbol{\varepsilon}'(t)\boldsymbol{\varepsilon}'^T(t)\right) + \lambda \mathrm{tr}\left(\boldsymbol{u}'(t)\boldsymbol{u}'^T(t)\right) \right\}. \end{aligned} \tag{38}$$

If $\boldsymbol{\mathcal{R}}(q^{-1})$ is chosen so that $\mathcal{L}_2 = \mathcal{L}_3$ equal zero, clearly the $\boldsymbol{\mathcal{T}}(q^{-1})$ that minimizes $\mathcal{L}$ is zero and $\boldsymbol{\mathcal{R}}$ is optimal.

Using Parseval's theorem, see e.g. [34, p. 395], the expressions (36) and trace rotation, we write

$$\begin{aligned} \mathcal{L}_3 = E\left\{ \mathrm{tr}\left(\boldsymbol{\varepsilon}(t)\boldsymbol{\varepsilon}'^T(t)\right) + \lambda \mathrm{tr}\left(\boldsymbol{u}(t)\boldsymbol{u}'^T(t)\right) \right\} \\ = \frac{1}{2\pi j} \oint_{|z|=1} \mathrm{tr}\Big(\lambda \mathbf{I}\boldsymbol{\mathcal{R}}(z^{-1})\varrho\mathbf{P}\boldsymbol{\mathcal{T}}_*(z) \\ + \boldsymbol{A}_*^{-1}(z)\boldsymbol{B}_*(z)\boldsymbol{V}_*(z)\boldsymbol{V}(z^{-1}) \\ \times \left(\boldsymbol{B}(z^{-1})\boldsymbol{A}^{-1}(z^{-1})\boldsymbol{\mathcal{R}}(z^{-1}) - \boldsymbol{D}(z^{-1})\right)\varrho\mathbf{P}\boldsymbol{\mathcal{T}}_*(z) \Big) \frac{dz}{z} \end{aligned} \tag{39}$$

where $\varrho\mathbf{P}$ is the covariance matrix of $\boldsymbol{r}(t)$. The expression above will equal zero if and only if the integrand has no poles on the closed unit disc [35, Appendix B].

Define the spectral factorization equation

$$\boldsymbol{\beta}_*(z)\boldsymbol{\beta}(z^{-1}) = \lambda \boldsymbol{A}_*\boldsymbol{A} + \boldsymbol{B}_*\boldsymbol{V}_*\boldsymbol{V}\boldsymbol{B}, \tag{40}$$

and combine this with equation (39) to obtain

$$\begin{aligned}\mathcal{L}_3 &= \frac{1}{2\pi j}\oint_{|z|=1} \mathrm{tr}\left(\left(\boldsymbol{A}_*^{-1}\left(\lambda \boldsymbol{A}_*\boldsymbol{A}\right)\boldsymbol{A}^{-1}\boldsymbol{\mathcal{R}}\right.\right.\\ &\left.\left.+\boldsymbol{A}_*^{-1}\boldsymbol{B}_*\boldsymbol{V}_*\boldsymbol{V}\boldsymbol{B}\boldsymbol{A}^{-1}\boldsymbol{\mathcal{R}} - \boldsymbol{A}_*^{-1}\boldsymbol{B}_*\boldsymbol{V}_*\boldsymbol{V}\boldsymbol{D}\right)\varrho\mathbf{P}\boldsymbol{\mathcal{T}}_*\right)\frac{dz}{z}\\ &= \frac{1}{2\pi j}\oint_{|z|=1}\mathrm{tr}\Big(\boldsymbol{A}_*^{-1}\left(\boldsymbol{\beta}_*\boldsymbol{\beta}\boldsymbol{A}^{-1}\boldsymbol{\mathcal{R}} - \boldsymbol{B}_*\boldsymbol{V}_*\boldsymbol{V}\boldsymbol{D}\right)\varrho\mathbf{P}\boldsymbol{\mathcal{T}}_*\Big)\frac{dz}{z}.\end{aligned} \tag{41}$$

The equation (40) will have a stably and causally invertible solution $\boldsymbol{\beta}(z^{-1})$ for any $\lambda > 0$, the case $\lambda = 0$ can, if needed, be handled with a small regularization. Since $\boldsymbol{A}(z^{-1})$ is a stably invertible polynomial matrix, all zeros of $\det(\boldsymbol{A}(z^{-1}))$ are contained within $|z| \leq 1$. The reciprocal, $\boldsymbol{A}_*^{-1}(z)$ therefore has no poles within the unit disc. The same goes for $\boldsymbol{\mathcal{T}}_*(z)$, since $\boldsymbol{\mathcal{T}}(z^{-1})$ is assumed stable. The covariance matrix $\mathbf{P}$ is independent of z. The spectral factor $\boldsymbol{\beta}(z^{-1})$ is minimum phase and hence stably invertible under general conditions. Choose the pre-compensation filter

$$\boldsymbol{\mathcal{R}} = \boldsymbol{A}\boldsymbol{\beta}^{-1}\boldsymbol{Q}, \tag{42}$$

and substitute (42) into (41). Setting the expression within the innermost parenthesis in the integrand of (41) equal to $z\boldsymbol{L}_*(z)$, where the factor z cancels the factor $^1/_z$ in (41) and $\boldsymbol{L}_*(z)$ is a polynomial matrix in positive powers of z only, this will guarantee that the integrand will have no poles in $|z| \leq 1$. This provides the Diophantine equation that guarantees an optimal polynomial matrix $\boldsymbol{Q}(q^{-1})$ in (42). Substituting the time domain operator q for z, we obtain

$$\boldsymbol{\beta}_*(q)\boldsymbol{Q}(q^{-1}) - \boldsymbol{B}_*(q)\boldsymbol{V}_*(q)\boldsymbol{V}(q^{-1})\boldsymbol{D}(q^{-1}) = q\boldsymbol{L}_*(q). \tag{43}$$

Here, $\boldsymbol{L}_*(q)$ contains polynomials in positive powers of q only. When (43) is satisfied,

$$\mathcal{L}_3 = \frac{1}{2\pi j}\oint_{|z|=1}\mathrm{tr}\left(\boldsymbol{A}_*^{-1}(z)\boldsymbol{L}_*(z)\varrho\mathbf{P}\boldsymbol{\mathcal{T}}_*(z)\right)dz = 0. \tag{44}$$

Equation (42) therefore yields the minimizing controller $\boldsymbol{\mathcal{R}}(q^{-1})$. The solution above is unique [35, Appendix B]. The equation (43) has a unique solution $\{\boldsymbol{Q}(q^{-1}), \boldsymbol{L}_*(q)\}$, see [17].

The controller (12) has generic numerator degrees $nn_{\boldsymbol{\mathcal{R}}} = n_{\boldsymbol{A}} + n_{\boldsymbol{Q}}$ where $n_{\boldsymbol{Q}} = n_{\boldsymbol{V}} + n_{\boldsymbol{D}}$. The degree of the non-causal polynomial $\boldsymbol{L}_*$ is $n_{\boldsymbol{L}} = \max(n_{\boldsymbol{B}} + n_{\boldsymbol{V}}, n_{\boldsymbol{\beta}}) - 1$. The controller denominator degree is $dn_{\boldsymbol{\mathcal{R}}} = n_{\boldsymbol{\beta}}$. Finally, $n_{\boldsymbol{\beta}} = \max(n_{\boldsymbol{A}}, n_{\boldsymbol{V}} + n_{\boldsymbol{B}})$.

Appendix B
Derivations of (30) in Section III-D

The solution to the problem (27) is found by tracing [5, Appendix B.] and [3]. In the following, the frequency bin index is omitted for the sake of brevity. The complex valued frequency domain variables can be vectorized into real valued matrices and vectors that fit the convex formalism.

Assuming a scalar $r(t)$ and defining the vectorized variables

$$\begin{aligned}\mathbf{R}_v &= \begin{bmatrix}\mathrm{Re}\left(\mathbf{R}\right)\\ \mathrm{Im}\left(\mathbf{R}\right)\end{bmatrix} \qquad \mathbf{M}_D = \begin{bmatrix}\mathrm{Re}\left(\mathbf{H}^H\mathbf{V}^H\mathbf{V}\mathbf{D}\right)\\ \mathrm{Im}\left(\mathbf{H}^H\mathbf{V}^H\mathbf{V}\mathbf{D}\right)\end{bmatrix}\\ \mathbf{M}_R &= \begin{bmatrix}\mathrm{Re}\left(\mathbf{H}^H\mathbf{V}^H\mathbf{V}\mathbf{H}\right) & -\mathrm{Im}\left(\mathbf{H}^H\mathbf{V}^H\mathbf{V}\mathbf{H}\right)\\ \mathrm{Im}\left(\mathbf{H}^H\mathbf{V}^H\mathbf{V}\mathbf{H}\right) & \mathrm{Re}\left(\mathbf{H}^H\mathbf{V}^H\mathbf{V}\mathbf{H}\right)\end{bmatrix},\end{aligned} \tag{45}$$

equation (27) can be posed as the convex optimization problem

$$\begin{aligned}\min_{\mathbf{R}_v}.\quad & \mathbf{R}_v^T\mathbf{M}_R\mathbf{R}_v - 2\mathbf{M}_D^T\mathbf{R}_v\\ \text{s.t.}\quad & \mathbf{R}_v^T\mathbf{R}_v - e_D \leq 0.\end{aligned} \tag{46}$$

Above, the term $\mathbf{D}^H\mathbf{V}^H\mathbf{V}\mathbf{D}$ of (27) is omitted as it is independent of both λ and $\mathbf{R}$. The Lagrangian, $\mathcal{L}$, becomes

$$\mathcal{L} = \mathbf{R}_v^T\mathbf{M}_R\mathbf{R}_v - 2\mathbf{M}_D^T\mathbf{R}_v + \lambda\left(\mathbf{R}_v^T\mathbf{R}_v - e_D\right), \tag{47}$$

and the optimal controller can be found by solving

$$\frac{\partial\mathcal{L}}{\partial\mathbf{R}_v} = 2\mathbf{R}_v^T\mathbf{M}_R - 2\mathbf{M}_D^T + 2\lambda\mathbf{R}_v^T = 0. \tag{48}$$

Provided $\mathbf{M}_R + \lambda\mathbf{I}$ is invertible (which it is, if $\lambda > 0$) the optimal $\mathbf{R}_v$ can now be found by solving

$$\mathbf{R}_v^{opt} = \left(\mathbf{M}_R^T + \lambda\mathbf{I}\right)^{-1}\mathbf{M}_D. \tag{49}$$

The concave dual function $\mathcal{G}(\lambda)$ is thus

$$\mathcal{G}(\lambda) = \mathcal{L}|_{\mathbf{R}_v^{opt}} = -\mathbf{M}_D^T\left(\mathbf{M}_R^T + \lambda\mathbf{I}\right)^{-1}\mathbf{M}_D - \lambda e_D. \tag{50}$$

Using the Schur complement, we can avoid a matrix inversion by expressing the maximization of (50) as

$$\begin{aligned}\max.\quad & \gamma\\ \text{s.t.}\quad & \lambda \geq 0\\ & \begin{bmatrix}\mathbf{M}_R^T + \lambda\mathbf{I} & \mathbf{M}_D\\ \mathbf{M}_D^T & -\lambda e_D - \gamma\end{bmatrix} \geq 0.\end{aligned} \tag{51}$$

This can be efficiently solved using e.g. the CVX toolbox for Matlab [36].

Appendix C
Experimental Evaluation Conditions

All measurements, both for the filter design, the simulation models and the verification measurement were made in a room of dimensions 2.6 by 4.5 by 5.8 meters. The main features of the room, in relation to acoustics, were a diffuser covering one wall and a thick curtain covering the opposite wall. Of the remaining walls, one was covered by a set of wall mounted shelves whereas the last wall was bare. The measurements were made above a sofa which was placed, facing the curtain, in the middle of the room, see Fig. 10.

Two sub woofers (speakers 2 and 7 in Fig. 10) and seven full range speakers were positioned around the sofa. The sound field was sampled in a 0.3 by 0.3 meters grid using microphones

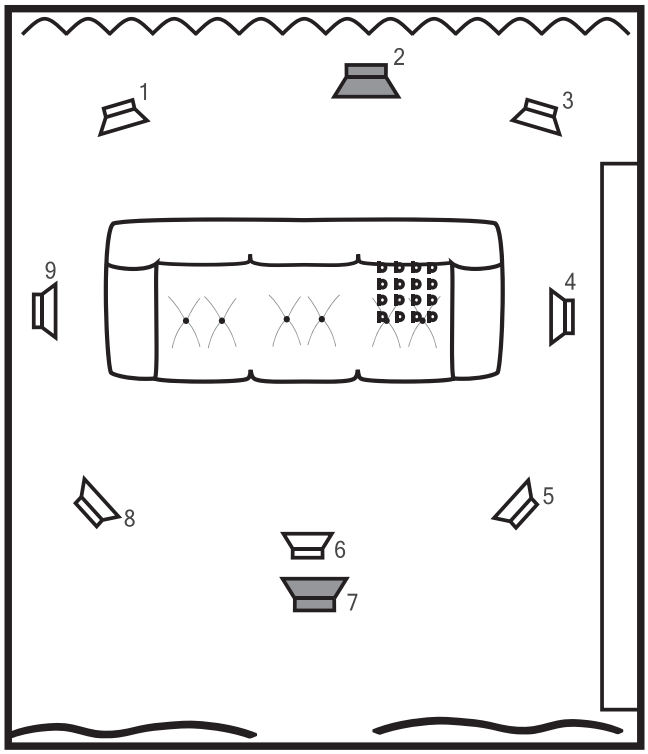

Fig. 10. The experimental setup. Shaded loudspeakers represent sub woofers. The 16 measurements on the left side of the sofa define the area in which the target sound field is to be reproduced.

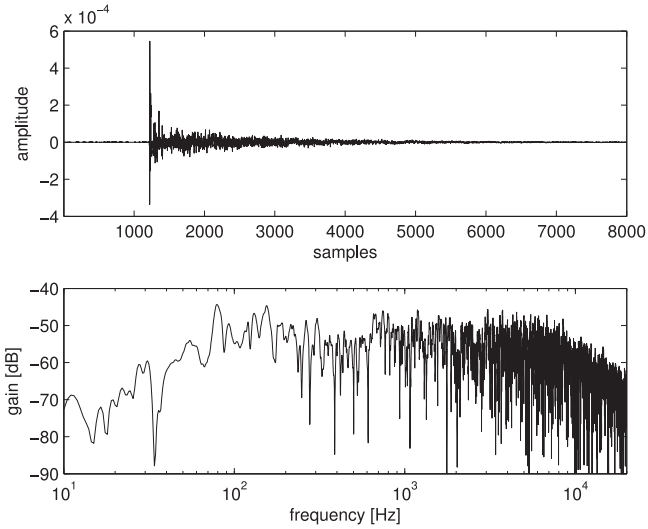

Fig. 11. The measured transfer function from one loudspeaker (number 6 in Fig. 10) to one microphone in the middle of the measurement grid measured at a sampling frequency of 44.1 kHz.

TABLE I
TIME AND FREQUENCY DOMAIN CONSTRAINTS OF THE EXPERIMENTALLY INVESTIGATED FILTER DESIGNS

Method	Power spectral gain constraint(s)
Constrained filter power (10)	$e_D \leq -22.5$ dB
Multiply constrained filter power (16)	$c_G \leq \begin{cases} -22.5 \text{ dB} & \text{for } 0 \leq f \leq \frac{1}{6} f_n \\ -22.5 \text{ dB} & \text{for } \frac{1}{6} f_n \leq f \leq \frac{2}{6} f_n \\ -22.5 \text{ dB} & \text{for } \frac{2}{6} f_n \leq f \leq \frac{3}{6} f_n \\ -22.5 \text{ dB} & \text{for } \frac{3}{6} f_n \leq f \leq \frac{4}{6} f_n \\ -22.5 \text{ dB} & \text{for } \frac{4}{6} f_n \leq f \leq \frac{5}{6} f_n \\ -22.5 \text{ dB} & \text{for } \frac{5}{6} f_n \leq f \leq \frac{6}{6} f_n \end{cases}$
Weighted criterion (26)	$e_{D_i} \leq -22.5$ dB
Causally unconstrained filter (27)	$e_{D_i} \leq -22.5$ dB

f_n refers to the temporal Nyquist frequency of the filter (22050 Hz).

spaced by $d_m = 0.1$ meters. The lowest spatial aliasing frequency on this grid is around 1200 Hz.[3] This has the practical implication that we cannot model the soundfield above 1200 Hz using the current measurement microphone separation and so results for the reproduced sound field above this frequency are valid only at the precise measurement positions. The full range speakers reliably reproduce sound between 60 Hz and 10 kHz (see Fig. 11) while speaker 2 does so between 30 Hz and 400 Hz and speaker 7 between 60 Hz and 200 Hz.

All measurements and experiments were performed with a sampling frequency of 44.1 kHz.

A. Modelling and Filter Design Parameters

Throughout the experiments, it is assumed that the driving noise, $\boldsymbol{r}(t)$, is scalar and white with zero mean and unit variance i.e. $l = 1$ and $\varrho = 1$.

The weighting filter $\boldsymbol{V}(q^{-1})$ for the error $\boldsymbol{\varepsilon}(t)$ of all investigated filter designs is here the unit matrix, assigning equal importance to all measurement points at all frequencies.

The target matrix $\boldsymbol{D}(q^{-1})$, which specifies the desired impulse responses at the measurement positions consists of ones, representing an ideal impulse, at delays corresponding to that of the propagation from loudspeaker 6 plus a modelling delay d of 0.01 s.

The step size of the search method described in Section III-C, iterating the matrix $\boldsymbol{U}(q^{-1})$, is here set to 10.

The constraints used for the implemented methods are also shown in Table I. In the case where different constraints are used for different frequency intervals, the values shown in the table are the maximally allowed average spectral density amplification, within the addressed frequency interval. The filters $\boldsymbol{\phi}_k(q^{-1})$ of Section III-B are, in the example, band pass filters that select the frequency bands for which we don't want the filter power gain to be greater than e_{Dk}. The band pass filtering will, however, mean that the constraint function with a narrow pass band would contain less power than one with a broader pass band if all other variables were the same. The pass band width independent constraint level is in Table I denoted c_G. The corresponding constraint level used in the optimization is

[3]The spatial Nyquist frequency is $f_n = {}^{c}/_{2d_m} = {}^{344}/_{0.2} = 1720$ Hz, for the longest possible propagation distance between two adjacent microphones, assuming a plane wave front. When using Kirkeby's rule of thumb [37] to have three measurement positions per wavelength to account for some near-field phenomena, the frequency limit becomes 1147 Hz.

$e_D = c_G i_f / i_{tot}$, where i_f is the bandwidth of the filtered out frequency interval of interest and i_{tot} is the width of the entire frequency interval.

ACKNOWLEDGMENT

The author would like to thank Prof. M. Sternad for providing invaluable insights, enthusiasm, and improvements upon the manuscript.

REFERENCES

[1] H. Fastl and E. Zwicker, *Psychoacoustics*, 3rd ed. Berlin, Germany: Springer, 2007.
[2] S. J. Elliott and J. Cheer, "Regularization and robustness of personal audio systems," 2011. [Online]. Available: http://eprints.soton.ac.uk/207989/1/Pub12685.pdf
[3] T. Betlehem and P. D. Teal, "A constrained optimization approach for multi-zone surround sound," in *Proc. IEEE Int. Conf. Acoust., Speech, Signal Process.*, 2011, pp. 437–440.
[4] Y. Huang, J. Benesty, and J. Chen, *Acoustic MIMO Signal Processing (Signals and Communication Technology)*. New York, NY, USA: Springer, 2006.
[5] S. Boyd and L. Vandenberghe, *Convex Optimization*. Cambridge, U.K.: Cambridge Univ. Press, 2004.
[6] T. Betlehem and C. Withers, "Sound field reproduction with energy constraint on loudspeaker weights," *IEEE Trans. Audio, Speech, Lang. Process*, vol. 20, no. 8, pp. 2388–2392, Oct. 2012.
[7] T. Michaeli and Y. C. Eldar, "Minimum MSE estimation with convex constraints," in *Proc. IEEE Int. Conf. Acoust., Speech, Signal Process.*, Apr. 2007, pp. III-1093–III-1096.
[8] T. Michaeli and Y. C. Eldar, "Constrained nonlinear minimum MSE estimation," in *Proc. IEEE Int. Conf. Acoust., Speech, Signal Process.*, Mar. 2008, pp. 3681–3684.
[9] S. Cecchi, A. Carini, and S. Spors, "Room response equalization: A review," *Appl. Sci.*, vol. 8, no. 1, 2017, Art. no. 16.
[10] A. J. Berkhout, "A holographic approach to acoustic control," *J. Audio Eng. Soc.*, vol. 36, no. 12, pp. 977–995, Dec. 1988.
[11] M. A. Gerzon, "Periphony: With-height sound reproduction," *J. Audio Eng. Soc.*, vol. 21, no. 1, pp. 2–10, Jan./Feb. 1973.
[12] O. Kirkeby and P. A. Nelson, "Digital filter design for inversion problems in sound reproduction," *J. Audio Eng. Soc.*, vol. 47, no. 7/8, pp. 583–595, Jul./Aug. 1999.
[13] E. I. Jury, *Sampled Data Control Systems*. Hoboken, NJ, USA: Wiley, 1958.
[14] V. Kučera, *Discrete Linear Control: The Polynomial Equation Approach*. Chichester, U.K.: Wiley, 1979.
[15] M. Sternad, M. Johansson, and J. Rutström, "Inversion of loudspeaker dynamics by polynomial LQ feedforward control," in *Proc. 3rd IFAC Symp. Robust Control Des.*, Prague, Czech Republic, 2000, pp. 693–697.
[16] T. Kailath, *Linear Systems*. Englewood Cliffs, NJ, USA: Prentice-Hall, 1980.
[17] M. Sternad and A. Ahlén, "LQ controller design and self-tuning control," in *Polynomial Methods in Optimal Control and Filtering*, K. Hunt, Ed. London, U.K.: Peregrinus, 1993, pp. 56–92.
[18] M. Johansson, L.-J. Brännmark, A. Bahne, and M. Sternad, "Sound field control using a limited number of loudspeakers," in *36th Int. Conf. Autom. Audio*, Dearborn, MI, USA, Paper no. 14, 2009.
[19] A. Barkefors, S. Berthilsson, and M. Sternad, "Extending the area silenced by active noise control using multiple loudspeakers," in *Proc. IEEE Int. Conf. Acoust., Speech, Signal Process.*, 2012, pp. 325–328.
[20] S. Berthilsson, A. Barkefors, L.-J. Brännmark, and M. Sternad, "Acoustical zone reproduction for car interiors using a MIMO MSE framework," in *Proc. AES 48th Int. Conf. Autom. Audio*, Sep. 2012, pp. 21–23.
[21] L. Lindbom, M. Sternad, and A. Ahlén, "Tracking of time-varying mobile radio channels—Part I: The Wiener LMS algorithm," *IEEE Trans. Commun.*, vol. 49, no. 12, pp. 2207–2217, Dec. 2001.
[22] A. Ahlén and M. Sternad, "Wiener filter design using polynomial equations," *IEEE Trans. Signal Process.*, vol. 39, no. 11, pp. 2387–2399, Nov. 1991.
[23] K. J. Hunt, Ed., *Polynomial Methods in Optimal Control and Filtering*. London, U.K.: Peregrinus, 1993.
[24] M. Sternad and A. Ahlén, "A novel derivation methodology for polynomial-LQ controller design," *IEEE Trans. Autom. Control*, vol. 38, no. 1, pp. 116–121, Jan. 1993.
[25] A. Barkefors, M. Sternad, and L.-J. Brännmark, "Design and analysis of linear quadratic Gaussian feedforward controllers for active noise control," *IEEE/ACM Trans. Audio, Speech, Lang. Process.*, vol. 22, no. 12, pp. 1777–1791, Dec. 2014.
[26] B. Bernhardsson and M. Sternad, "Feedforward control is dual to deconvolution," *Int. J. Control*, vol. 57, no. 2, pp. 393–405, 1993.
[27] K. Öhrn, A. Ahlén, and M. Sternad, "A probabilistic approach to multivariable robust filtering and open-loop control," *IEEE Trans. Autom. Control*, vol. 40, no. 3, pp. 405–418, Mar. 1995.
[28] V. Kučera, *Analysis and Design of Discrete Linear Control Systems*. Prague, Czech Republic: Academia, 1991.
[29] M. F. Simón Gálvez, "Design of an array-based aid for the hearing impaired," Ph.D. dissertation, Univ. Southampton, Southampton, U.K., 2014.
[30] F. Zhang, *The Schur Complement and Its Applications*, vol. 4. New York, NY, USA: Springer, 2006.
[31] L.-J. Brännmark and A. Ahlén, "Spatially robust audio compensation based on SIMO feedforward control," *IEEE Trans. Signal Process.*, vol. 57, no. 5, pp. 1689–1702, May 2009.
[32] L.-J. Brännmark, A. Bahne, and A. Ahlén, "Compensation of loudspeaker-room responses in a robust MIMO control framework," *IEEE Trans. Audio, Speech, Lang. Process.*, vol. 21, no. 6, pp. 1201–1216, Jun. 2013.
[33] L.-J. Brännmark, "Robust audio precompensation with probabilistic modeling of transfer function variability," in *Proc. IEEE Workshop Appl. Signal Process. Audio Acoust.*, New Paltz, NY, USA, Oct. 2009, pp. 193–196.
[34] K. J. Åström and B. Wittenmark, *Computer-Controlled Systems: Theory and Design*. Englewood Cliffs, NJ, USA: Prentice-Hall, 1997.
[35] C. Tidestav, "The multivariable decision feedback equalizer: Multiuser detection and interference rejection," Ph.D. dissertation, , Uppsala Univ., Uppsala, Sweden, 1999. [Online]. Available: http://www.signal.uu.se/Publications/pdf/a993.pdf
[36] M. Grant and S. Boyd, "CVX: Matlab software for diciplined convex programming," 2017. [Online]. Available: http://cvxr.com/cvx/
[37] O. Kirkeby, "Reproduction of acoustic fields," Ph.D. dissertationUniv. Southampton, Southampton, U.K., 1995.

Simon Widmark (formerly Berthilsson) (S'12) received the M.Sc. degree in engineering physics from Uppsala University, Uppsala, Sweden, in 2010. He has been with the Signals and Systems Group, Uppsala University, Uppsala, Sweden, and Dirac Research AB, Uppsala, Sweden, where he has been working toward the Ph.D. degree since 2011.

His research focuses on sound field synthesis with applications in active noise control and personal audio, primarily in car environments.